

MAX-DOAS O₄ measurements: A new technique to derive information on atmospheric aerosols:

2. Modeling studies

U. Frieß,¹ P. S. Monks,² J. J. Remedios,² A. Rozanov,³ R. Sinreich,¹ T. Wagner,¹ and U. Platt¹

Received 24 August 2005; revised 30 January 2006; accepted 7 April 2006; published 19 July 2006.

[1] A new retrieval algorithm for the determination of aerosol properties using Multi-Axis Differential Optical Absorption Spectroscopy (MAX-DOAS) measurements based on nonlinear optimal estimation is presented. Using simulated MAX-DOAS measurements of the optical depth of the collision complex of oxygen (O₄) as well as the variation of the intensity of diffuse skylight measured at different viewing directions and wavelengths, the capability of this measurement technique to derive the aerosol extinction profile as well as information on the phase function and single scattering albedo is demonstrated. The information content, vertical resolution and retrieval errors under various atmospheric conditions are discussed. Furthermore, it is demonstrated that the assumption of a smooth variation of the aerosol properties between successive measurements can be used to improve the quality of the retrieval by applying a Kalman smoother. The results of these model studies suggest that the achievable precision of MAX-DOAS measurements of the aerosol total optical depth is better than 0.01 and thus comparable with established methods of aerosol detection by Sun photometers (e.g., within the AERONET network) over a wide range of atmospheric conditions. Moreover, MAX-DOAS measurements contain information on the vertical profile of the aerosol extinction, and can be performed with relatively simple, robust and self-calibrating instruments.

Citation: Frieß, U., P. S. Monks, J. J. Remedios, A. Rozanov, R. Sinreich, T. Wagner, and U. Platt (2006), MAX-DOAS O₄ measurements: A new technique to derive information on atmospheric aerosols: 2. Modeling studies, *J. Geophys. Res.*, *111*, D14203, doi:10.1029/2005JD006618.

1. Introduction

[2] Aerosols play an important role in the physics and chemistry of the atmospheric system. Scattering and absorption of radiation by aerosols, as well as various indirect effects altering the optical properties of clouds, have an impact on the Earth's radiation budget and hence on climate. The lack of knowledge on the anthropogenic contribution to the atmospheric aerosol load represents the highest uncertainty in climate forcing assessments [Charlson *et al.*, 1992; Tegen and Lacis, 1996; Hansen *et al.*, 1997; Houghton *et al.*, 2001].

[3] This paper represents the second in a series of papers on Multi-Axis Differential Optical absorption spectroscopy (MAX-DOAS) measurements as a new technique to derive information on atmospheric aerosols. The first part by

Wagner *et al.* [2004] has investigated the potential of MAX-DOAS measurements to derive information on aerosol properties in detail using observations made during the FORMAT II campaign. On the basis of the interpretation of MAX-DOAS measurements of the optical depth of the oxygen collision complex (O₄) using a Monte Carlo radiative transfer model, it has been concluded that such measurements yield substantial information on the vertical distribution of aerosols. Furthermore, it has been shown that further information on aerosol properties can be derived if the intensity and the amount of inelastic scattering (quantified by the so-called Ring effect) are considered. In particular, the variation of intensity with elevation and solar zenith angle has been suggested to yield information on the amount of absorbing aerosols.

[4] The underlying measurement technique, Differential Optical Absorption Spectroscopy (DOAS) of scattered solar radiation in the UV/Vis spectral region, is a widely used technique for the detection of atmospheric trace gases [Platt, 1994]. DOAS measurements provide information on the integrated concentration of atmospheric absorbers by detecting their wavelength dependent absorption structure. Ground-based DOAS observations of the skylight scattered at zenith during twilight have been performed at

¹Institute for Environmental Physics, University of Heidelberg, Heidelberg, Germany.

²Space Research Centre, University of Leicester, Leicester, UK.

³Institute of Environmental Physics, University of Bremen, Bremen, Germany.

various locations. Since, in twilight geometry, the bulk of scattering takes place in the lower stratosphere and upper troposphere, zenith-sky DOAS measurements are characterized by a high sensitivity to stratospheric absorbers, while the sensitivity to absorbers close to the surface is relatively low. Ground-based MAX-DOAS, a technique that has found a growing number of applications in recent years, takes advantage of the length of the light path through the lower troposphere being significantly increased when observing scattered light from a line of sight close to the horizon. Sequential or simultaneous observations of scattered light from a variety of viewing angles have been shown to yield significant information about the vertical profile of trace gases (e.g., BrO, IO, NO₂, HCHO) located near the surface [Hönninger and Platt, 2002; Leser et al., 2003; Bobrowski et al., 2003; van Roozendaal et al., 2003; Wittrock et al., 2004; Hönninger et al., 2004].

[5] In this paper a retrieval algorithm for the determination of vertical profiles and optical properties of atmospheric aerosols based on MAX-DOAS measurements of O₄ and intensity is presented. First, a review of the MAX-DOAS measurement principles is given in section 2. A detailed study of the sensitivity of MAX-DOAS observations on aerosols is presented in section 3. Finally, the retrieval algorithm is described and a number of sensitivity studies including the discussion of random and systematic errors is presented in section 4.

2. MAX-DOAS Measurements of O₄

[6] The detection of trace gases in the atmosphere using the DOAS method is based on the Lambert-Beer law, which describes the relationship between the incident light intensity at the location of the light source (or, in case of scattered light, at the top of the atmosphere) and the transmitted intensity at the location of an observer. Assuming that only a single absorber is present in the atmosphere and that the dependence of the absorption cross section on pressure and temperature can be neglected, the Lambert-Beer law can be written in a simplified form as

$$I(\lambda) = I_0(\lambda) \cdot \exp\left(-\int_0^L (\sigma(\lambda)\rho(s) + k_r(\lambda, s) + k_m(\lambda, s))ds\right), \quad (1)$$

with $I_0(\lambda)$ and $I(\lambda)$ being the incident and transmitted intensity, respectively, at wavelength λ , L the length of the light path, $\sigma(\lambda)$ the absorption cross section of the trace gas, and $\rho(s)$ the trace gas concentration at location s . $k_r(\lambda, s)$ and $k_m(\lambda, s)$ are the extinction coefficients for Rayleigh scattering on air molecules and Mie scattering on particles, respectively.

[7] The DOAS method relies on the fact that Rayleigh and Mie extinction cause only broad-banded structures in the spectra and can be approximated by a polynomial of low order. This approximation allows the determination of the slant column density (SCD), i.e., the integrated concentration along the light path,

$$S = \int_0^L \rho(s)ds \quad (2)$$

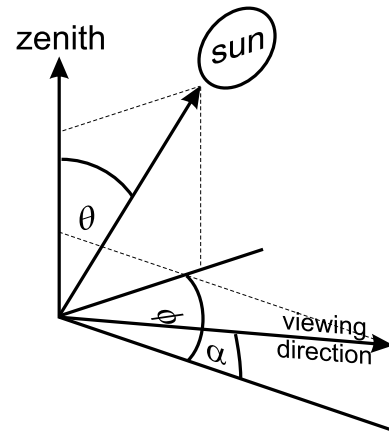


Figure 1. Definition of the viewing geometry of a MAX-DOAS measurement.

simultaneously for several absorbers by using a least squares algorithm. Alternatively, the strength of absorption due to a particular trace gas can be quantified by the optical depth

$$\tau(\lambda) = \sigma(\lambda) \cdot S = -\ln\left(\frac{I(\lambda)}{I'_0(\lambda)}\right), \quad (3)$$

where I'_0 is the intensity that would be observed in the absence of the absorber, but with all other atmospheric parameters left unchanged.

[8] The SCD S and the corresponding optical depth τ depend on the observation geometry, which is defined by the line of sight (LOS) of the observer as well as by the position of the Sun relative to the LOS. The angles specifying the observation geometry are summarized in a vector $\Omega = (\alpha, \theta, \phi)$, with α being the elevation angle (angle between the line of sight and the horizon), θ the solar zenith angle, and ϕ the relative azimuth angle, as illustrated in Figure 1.

[9] The air mass factor (AMF) a is defined as the ratio between slant column density S and the vertically integrated trace gas concentration, which can be written in terms of the optical depth as

$$a(\lambda, \Omega) = \frac{\tau(\lambda, \Omega)}{\tau_V(\lambda)}, \quad (4)$$

with $\tau_V(\lambda) = \int \tau(\lambda, z) dz$ being the vertically integrated optical depth. The AMFs simulated by a radiative transfer model can be compared to a simple geometrical approximation of the air mass factor for a trace gas located entirely in the lower troposphere as derived by Hönninger et al. [2004],

$$\xi(\alpha) = \frac{1}{\sin(\alpha)}. \quad (5)$$

[10] The primary quantity measured by DOAS is not the absolute optical depth τ from equation (3), but the differential optical depth (DOD) $\Delta\tau$ relative to a reference spectrum,

$$\Delta\tau(\lambda, \Omega) = \tau(\lambda, \Omega) - \tau_{ref}(\lambda), \quad (6)$$

where $\tau_{ref}(\lambda) \equiv \tau(\lambda, \Omega_{ref})$ is the optical depth measured with the observation geometry Ω_{ref} (note that the term “differential” is used here for the difference between optical depths at different observation geometries, while it usually refers to the difference in optical depths at different wavelengths). Only relative changes in optical depth can be detected because the measured spectrum I is usually divided by a reference spectrum I_{ref} rather than by an extraterrestrial spectrum I_0 (see equation (1)). Here a reference spectrum measured in zenith with a short time span between the acquisitions of reference and measurement spectrum is chosen to ensure that no significant change in the aerosol extinction profile occurs between both observations. This avoids any difficulties in the interpretation of the differential optical depths caused by the temporal variability of the aerosol extinction profile.

[11] The length of the light path through the atmosphere and thus the observed optical depth of a trace gas will depend on the amount and optical properties of aerosol particles present in the atmosphere. Assuming the properties of atmospheric aerosols and therefore the light path distribution is known, it is possible to retrieve information on the vertical profile of atmospheric trace gases by measuring their optical depth at different viewing directions. However, a complementary way of retrieving information on the state of the atmosphere is to use measurements of the optical depths τ_i along different lines of sight Ω_i and/or at different wavelengths λ_i for an absorber with known vertical profile $\rho(z)$. This provides information on the vertical distribution and optical properties of atmospheric aerosols [Wagner *et al.*, 2002]. The oxygen collision complex O₄ is ideally suited for this approach. The concentration of O₄ is proportional to the square of the O₂ concentration and therefore exponentially decreasing with altitude with a scale height of approximately 4 km. Since the bulk concentration of O₄ is located close to the surface, the optical depth of O₄ is very sensitive to changes in the light path distribution at low altitudes. O₄ has numerous absorption bands in the UV/Vis spectral region [Greenblatt *et al.*, 1990]. It is easily detectable with high accuracy by DOAS instruments, and measurements at different O₄ absorption bands yield information on the wavelength dependence of the aerosol extinction.

[12] A further quantity which contains information on the aerosol extinction profile as well as optical and microphysical properties is the intensity of scattered light measured by MAX-DOAS instruments [Wagner *et al.*, 2004]. However, DOAS instruments are usually not absolutely radiometrically calibrated, which means that only relative changes in the intensity as a function of observation geometry can be inferred. The comparison of intensities measured at different wavelengths (usually referred to as color index) would yield considerable information on the wavelength dependence of the aerosol extinction. However, the instrument response function (i.e., the sensitivity of the spectrograph/detector system as a function of wavelength) of a DOAS instrument is usually not known, which means that only changes in the intensity at the same wavelength can be derived with high accuracy from MAX-DOAS instruments.

[13] In this work, the intensity index \tilde{I} is defined as the intensity (or detector signal) relative to a reference spectrum measured at the same wavelength,

$$\tilde{I}(\lambda, \Omega) = \frac{I(\lambda, \Omega)}{I_{ref}(\lambda)}, \quad (7)$$

where $I(\lambda, \Omega)$ is the intensity measured at wavelength λ and with the observation geometry Ω , and $I_{ref}(\lambda) \equiv I(\lambda, \Omega_{ref})$ is the reference intensity measured at the same wavelength but with the viewing geometry Ω_{ref} (usually a zenith sky spectrum).

3. Sensitivity of MAX-DOAS O₄ Measurements to Atmospheric Parameters and Viewing Geometry

[14] In this section, the sensitivity of the quantities measured by a DOAS system (O₄ DOD and intensity index) to atmospheric parameters and the viewing geometry is discussed. Simulations of MAX-DOAS measurements have been performed using the SCIATRAN radiative transfer model [Roazanov *et al.*, 2005] (<http://www.iup.physik.uni-bremen.de/sciatran>). In this study, SCIATRAN was run in the approximative spherical mode which is based on the combined differential-integral CDI approach [Roazanov *et al.*, 2000, 2001]. In this mode, the radiative transfer equation is solved in its integral form in a spherical atmosphere properly accounting for the single scattering and using an approximation for the multiply scattered radiation. The refraction was also accounted for. O₄ AMFs and relative intensities have been simulated using different viewing geometries based on aerosol profiles for a midlatitude summer standard atmosphere taken from the LOWTRAN library. In this study, the AMFs of O₄ are modeled at the maxima of four O₄ absorption lines in the UV/Vis, centered around 359.7, 477.0, 577.4 and 629.8 nm. The studies presented here use the SCIATRAN aerosol parameterization, which allows the specification of an aerosol extinction profile at a reference wavelength (which has been set to 550 nm) on an arbitrary vertical grid. Here a vertical resolution of 200 m in the lowermost 4 km of the atmosphere, and 250 m between 4 and 5 km is used. The vertical resolution between 5 and 80 km varies from 500 m to 2 km, but is not important for this study which focuses on the lower troposphere only. Aerosol phase function and single scattering albedo can be defined implicitly in SCIATRAN by choosing the composition of a mixture of different aerosol types (e.g., water-soluble, sea salt, sulfate, dust, soot and mineral aerosols with different size distributions). The wavelength-dependent phase function and single scattering albedo are calculated by SCIATRAN using an internal Mie database based on Henyey-Greenstein phase functions [Henyey and Greenstein, 1941].

3.1. Dependency on Elevation Angle

[15] The modeled O₄ AMFs a at the absorption bands centered around 360, 477, 577 and 630 nm are shown in Figure 2 as a function of geometrical AMF ξ and aerosol vertical optical depth (AOD) $\tau_A(\lambda) = \int k_m(z) dz$. The calculations were performed for an aerosol extinction profile linearly decreasing from the surface up to an altitude of 3 km at an SZA of 85° and an azimuth angle of 90°. The dashed

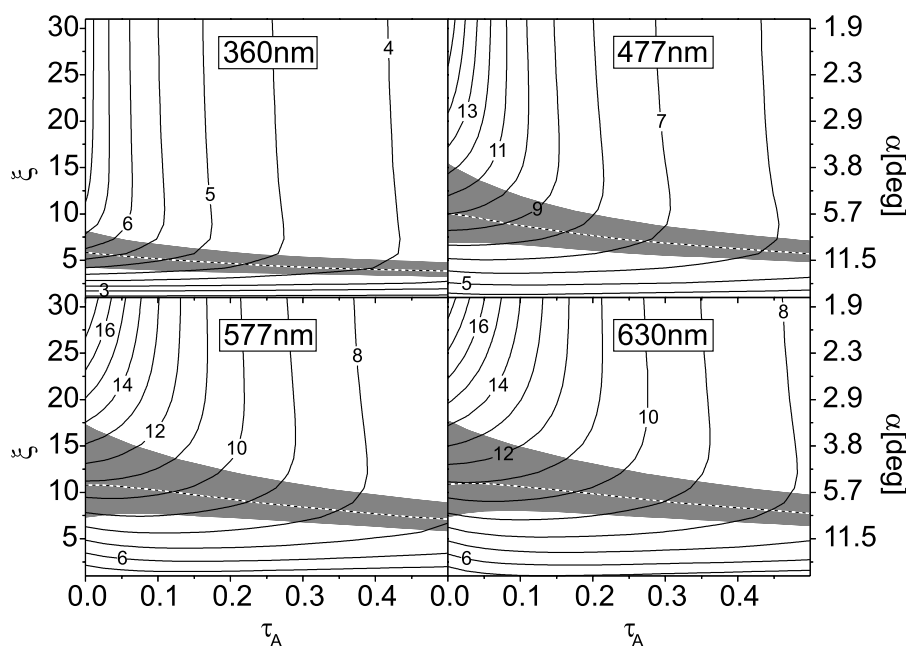


Figure 2. Contour plots showing the modeled O₄ AMF a at the 360, 477, 577, and 630 nm absorption bands as a function of geometrical AMF $\xi = 1/\sin(\alpha)$ (the elevation angle α is shown at the right-hand axis) and AOD τ_A . The dashed isolines indicate where the modeled AMF equals the geometrical AMF, and the gray areas indicate where ξ and a agree within 20%. For further details, see text.

isolines indicate where $a = \xi$, and the gray areas show regions where modeled and geometrical AMF agree within 20%. The geometrical AMF from equation (5) is only valid over a very small range of elevations at the 360 nm absorption band, but yields a good approximation for $4 < \xi < 15$ (corresponding to elevations between 3.8° and 14.5°) at higher wavelengths.

[16] For a constant AOD, the O₄ AMF (and thus the atmospheric light path) increases with ξ at high elevation angles as expected from the geometrical approximation, but remains almost constant at high geometrical air mass factors (low elevations), and even decreases with increasing ξ for high AODs. These shorter light paths at low elevation angles are caused by a reduction of the visibility when pointing closer to the horizon, which leads to a reduction in the average scattering distance along the line of sight.

[17] The variation of the relative intensity with geometrical air mass factor and AOD shown in Figure 3 is characterized by a complex pattern. A larger amount of scattering by particles leads to an increase in intensity index with geometrical air mass factor (decreasing elevation) before it reaches a maximum at a value of ξ which depends on the AOD, and decreases again when pointing closer to the horizon because extinction of light by aerosols becomes dominant at low elevations. It is worth noting that the general decrease in relative intensity with AOD does not imply that the absolute intensity diminishes with increasing aerosol load (the opposite is generally true), but merely that the ratio between the intensities measured off axis and in the zenith becomes smaller (i.e., the increase in brightness owing to an increase in aerosols is stronger in the zenith than close to the horizon).

[18] The sensitivities of both the O₄ AMF and the intensity index vary strongly with wavelength. The variation of the O₄ AMF as a function of elevation angle is weaker at shorter wavelengths, while the converse is true for the intensity index, for which the variation with elevation angle is strongest at 360 nm.

3.2. Dependency on Azimuth Angle

[19] By measuring scattered sunlight at different azimuth angles, the variation in scattering angle between Sun and observer provides information on the aerosol phase function. The variation of the intensity with azimuth is used for the retrieval of aerosol size distribution and complex refractive index by sky radiometers within the AERONET network [Dubovik *et al.*, 2000; Dubovik and King, 2000]. To quantify the sensitivity of MAX-DOAS measurements at different elevations to the optical properties of aerosol particles, a mixture of water-soluble aerosols (represented in SCIATRAN as a mixture of sulfates nitrates, and other water-soluble compounds) with high single scattering albedo and of strongly absorbing soot particles has been modeled with varying soot fraction q . The aerosol extinction (at the reference wavelength of 550 nm) was kept constant during these calculations with a linearly decreasing profile from the ground to an altitude of 3 km and an AOD of 0.29, corresponding to a visibility of 25 km (the visibility with respect to aerosols is defined here as 3.9 divided by the surface aerosol extinction coefficient at 550 nm [Seinfeld and Pandis, 1998]). The variation of the 477 nm O₄ AMF and intensity index with azimuth angle and fraction of soot aerosols q is shown in Figure 4. The calculations have been performed for a solar zenith angle of 60° and an elevation angle of 30° (i.e., in the solar almucantar where

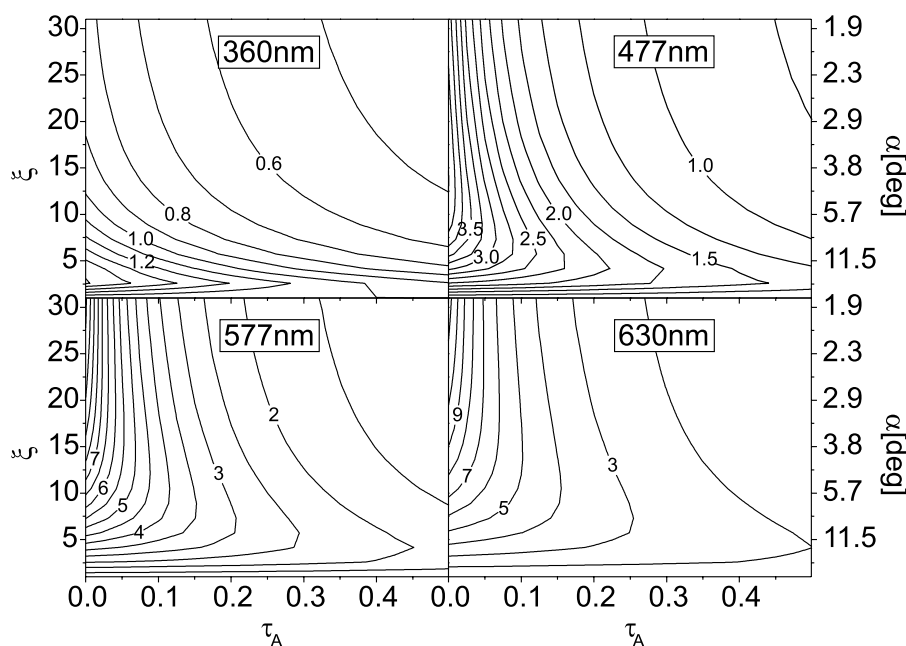


Figure 3. As in Figure 2, but for isolines of the intensity index (ratio of the intensity in off-axis viewing direction and the intensity in zenith direction at the same SZA.)

$\alpha = 90^\circ - \Theta$). The O₄ AMF is generally smaller when pointing toward the Sun ($\phi = 0^\circ$) than when pointing away from the Sun ($\phi = 180^\circ$). This is owing to the shorter light paths caused by the strong preference of forward scattering by aerosol particles. The O₄ AMF as a function of azimuth angle changes significantly with the amount of absorbing aerosols, with a smaller difference between the AMFs in forward and backward direction at higher values of q . The AMFs decrease with increasing q as a result of the preference of shorter light paths in a stronger absorbing atmosphere.

[20] As expected, the intensity index decreases with increasing soot fraction owing to an increase in absorption of radiation. The sensitivity of the intensity index to the aerosol composition is particularly high for small azimuth angles. Thus best sensitivity for the aerosol composition can be achieved by measuring in the aureole region of the Sun ($\phi < 10^\circ$), which requires a small field of view of the instrument and a high pointing accuracy.

[21] It can be concluded that measurements at different azimuth angles provide significant information on the

optical properties of atmospheric aerosols. The measurements are particularly sensitive to the aerosol composition when observing light from the aureole region of the Sun.

3.3. Dependency on Surface Albedo

[22] The surface albedo has a significant impact on MAX-DOAS measurements of O₄ and more particularly of the intensity. The dependence appears to be strongest at low elevation angles. This is illustrated in Figure 5 which shows the dependence of the O₄ AMF and the intensity index on albedo and elevation angle, calculated at a wavelength of 477 nm for a visibility of 25 km at an SZA of 85° and an azimuth angle of 90°. For a geometrical air mass factor of $\xi = 20$ (corresponding to an elevation angle of $\alpha \approx 3^\circ$), the relative intensity increases by $\approx 50\%$ when varying the albedo between 0 (black surface) and 1 (entirely reflective surface). The corresponding change in the O₄ AMF is much smaller ($\approx 5\%$).

[23] The effect of the albedo on MAX-DOAS measurements can be very subtle in the case of measurements over

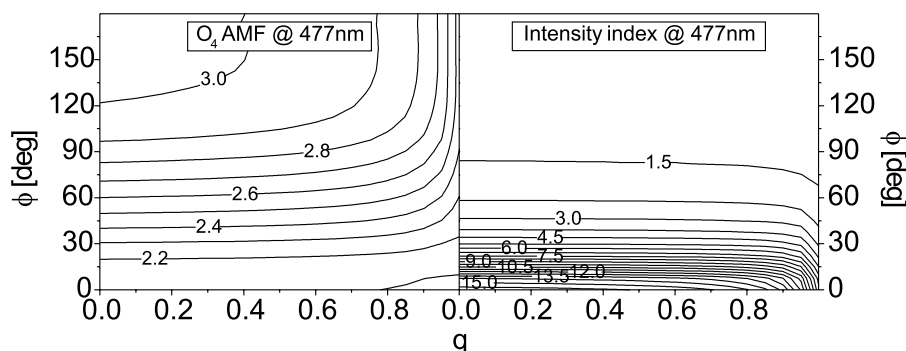


Figure 4. Contour plots of the (left) modeled O₄ AMF and (right) relative intensity at 477 nm as a function azimuth angle ϕ and fraction of soot aerosols q .

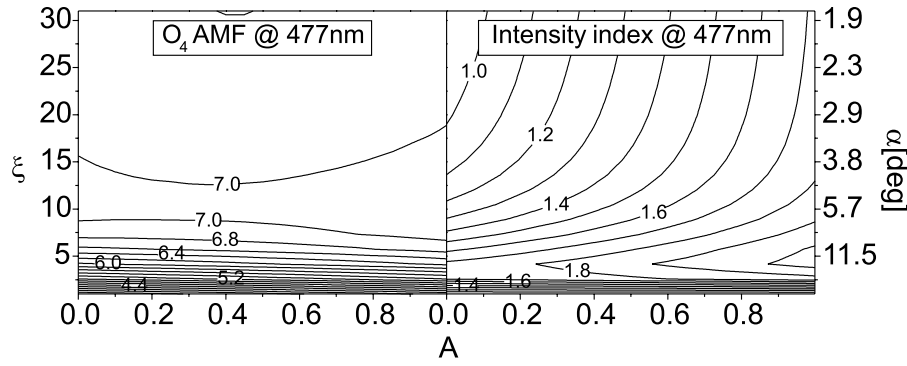


Figure 5. Contour plots of the (left) modeled O₄ AMF and (right) relative intensity at 477 nm as a function of geometrical air mass factor $\xi = 1/\sin(\alpha)$ and surface albedo A .

inhomogeneous terrain, since radiation reflected from areas with varying reflectivity contributes to the scattered light, and the contribution from different surfaces changes with elevation and solar zenith angle. It is therefore problematic to use a fixed albedo in a retrieval algorithm. Instead, the albedo should be a retrieval parameter, as described below in section 4.2.

4. Retrieval of Aerosol Properties Using Optimal Estimation

[24] In general, the estimation of the state of the atmosphere \mathbf{x} from a set of remote sensing measurements \mathbf{y} represents an inverse problem of the form

$$\mathbf{y} = \mathbf{F}(\mathbf{x}, \mathbf{b}) + \epsilon. \quad (8)$$

The m -element measurement vector \mathbf{y} is a function $\mathbf{F}(\mathbf{x}, \mathbf{b})$ of the n -element state vector \mathbf{x} , with \mathbf{x} containing quantities describing the state of the atmosphere. The forward model parameters \mathbf{b} are values quantifying further properties of the system which are not retrieved, for example, are assumed to be known with sufficient accuracy. The vector ϵ describes the random and systematic errors of the measurement. The forward model operator $\mathbf{F}(\mathbf{x}, \mathbf{b})$ is a vector valued function of the state vector, usually implemented as a numerical model which represents the physics of the system which is in our case the SCIATRAN radiative transfer model.

[25] Optimal estimation is a widely used technique for solving inverse problems in atmospheric remote sensing applications [Rodgers, 1990, 2000]. In particular, it has been applied to ground-based DOAS measurements of scattered and direct sunlight [e.g., Preston *et al.*, 1997; Hendrick *et al.*, 2004; Schofield *et al.*, 2004] for the retrieval of vertical trace gas profiles, such as NO₂ and BrO. The application of the optimal estimation method to DOAS observations is described in detail elsewhere [e.g., Haley *et al.*, 2004; Hoogen *et al.*, 1999] and is therefore only briefly summarized here.

[26] In case of a nonlinear problem, the maximum a posteriori (MAP) solution $\hat{\mathbf{x}}$ of an inverse problem, as given by equation (8), can be determined iteratively using the Gauss-Newton method,

$$\mathbf{x}_{i+1} = \mathbf{x}_i + (\mathbf{S}_a^{-1} + \mathbf{K}_i^T \mathbf{S}_\epsilon^{-1} \mathbf{K}_i)^{-1} \cdot [\mathbf{K}_i^T \mathbf{S}_\epsilon^{-1} (\mathbf{y} - \mathbf{F}(\mathbf{x}_i)) - \mathbf{S}_a^{-1} (\mathbf{x}_i - \mathbf{x}_a)]. \quad (9)$$

The a priori state vector \mathbf{x}_a represents an estimate of the state of the system before the measurement has been made, a quantity that can be derived, for example, from climatological means or from other independent sources. The a priori provides additional constraints on the atmospheric state in case of underdetermined problems. \mathbf{S}_ϵ and \mathbf{S}_a are the covariance matrices of measurement and a priori, respectively. The weighting function matrix (Jacobi matrix) $\mathbf{K}_i = \mathbf{K}(\mathbf{x}_i)$ is the matrix of partial derivatives of the forward model with respect to the state vector, which describes the sensitivity of the measurement to perturbations in the state vector; that is, the elements of the weighting functions are

$$K_{jk} = \frac{\partial F_j(\mathbf{x})}{\partial x_k}. \quad (10)$$

[27] In case of aerosol retrieval from MAX-DOAS measurements, the calculation of the weighting function is the most time consuming step in the retrieval and needs to be performed in each iteration. A slightly modified version of equation (9) based on the method of Levenberg [1944] and Marquardt [1963] with a faster convergence rate is used here. Details are given by Press *et al.* [1988].

[28] The error of the retrieved state vector is quantified by the retrieval covariance matrix,

$$\hat{\mathbf{S}} = (\mathbf{K}^T \mathbf{S}_\epsilon^{-1} \mathbf{K} + \mathbf{S}_a^{-1})^{-1}, \quad (11)$$

which can be written as the sum of two independent error sources, $\hat{\mathbf{S}} = \mathbf{S}_s + \mathbf{S}_m$. The smoothing error \mathbf{S}_s quantifies the error owing to the limited vertical resolution of the retrieval, while the retrieval noise \mathbf{S}_m represents the uncertainty caused by the measurement errors. Note that the retrieval covariance from equation (11) does not include forward model errors and model parameter errors. These error components are discussed in section 4.8.

4.1. Information Aspects

[29] An important quantity for the characterization of a retrieval is the sensitivity of the retrieved state $\hat{\mathbf{x}}$ to the true state \mathbf{x} , which is given by the averaging kernel matrix

$$\mathbf{A} \equiv \frac{\partial \hat{\mathbf{x}}}{\partial \mathbf{x}} = (\mathbf{S}_a^{-1} + \mathbf{K}^T \mathbf{S}_\epsilon^{-1} \mathbf{K})^{-1} \mathbf{K}^T \mathbf{S}_\epsilon^{-1} \mathbf{K} \quad (12)$$

in the sense that, for a noise free measurement, the retrieved state vector is a smoothed version of the true atmospheric state,

$$\hat{\mathbf{x}} = \mathbf{x}_a + \mathbf{A}(\mathbf{x} - \mathbf{x}_a). \quad (13)$$

[30] In the case of the retrieval of atmospheric profiles, this means that the averaging kernels (rows of \mathbf{A}) quantify how the true profile is averaged in order to reproduce the retrieval at a particular altitude level. The averaging kernels therefore provide a measure for the vertical resolution of the measurement and the sensitivity of the retrieval to the true state at particular altitudes. The averaging kernel matrix of an ideal retrieval would be the unit matrix ($\mathbf{A} = \mathbf{I}$), yielding $\hat{\mathbf{x}} = \mathbf{x}$.

[31] The number of independent pieces of information that can be measured is quantified by the degrees of freedom for signal,

$$d_s = \text{tr}(\mathbf{A}). \quad (14)$$

The vertical resolution of the retrieval can be quantified using the spread function as defined by *Backus and Gilbert* [1970],

$$s(z) = 12 \frac{\int (z - z')^2 A^2(z, z') dz'}{(\int A(z, z') dz')^2}, \quad (15)$$

which provides an estimate of the width of the averaging kernel at altitude z [*Rodgers, 2000*].

4.2. Applying Optimal Estimation to MAX-DOAS

[32] In case of the retrieval of atmospheric aerosol properties using MAX-DOAS measurements of scattered sunlight, the measurements consist of the DODs of O₄ and the intensities relative to a reference spectrum observed at m different combinations (λ_j, Ω_j) of wavelengths λ_j and lines of sight Ω_j ($j = 1, \dots, m$), which can be summarized in the measurement vector as

$$\mathbf{y} = \begin{pmatrix} \Delta\tau(\lambda_1, \Omega_1) \\ \vdots \\ \Delta\tau(\lambda_m, \Omega_m) \\ \tilde{I}(\lambda_1, \Omega_1) \\ \vdots \\ \tilde{I}(\lambda_m, \Omega_m) \end{pmatrix}. \quad (16)$$

[33] Here it is assumed that both the O₄ DODs and the intensity indices are determined relative to a zenith sky measurement at the same wavelength and solar zenith angle.

[34] The quantities to be retrieved from the MAX-DOAS measurements are as follows.

[35] 1. The aerosol extinction profile is represented by the extinction coefficients $k_i = k(z_i)$ ($i = 1, \dots, n$) at n discrete layers centered around the altitudes z_i .

[36] 2. Parameters q_j ($j = 1, \dots, r$) describe the optical or microphysical properties of aerosols. These can be parameters representing the phase function (e.g., the asymmetry parameter when using a Henyey-Greenstein phase function)

and the single scattering albedo, or the particle size distribution and complex refractive index.

[37] 3. The wavelength-dependent surface albedo is given by $A_k = A(\lambda_k)$ ($k = 1, \dots, s$). The reasons for retrieving the albedo (rather than using predetermined values) have already been discussed in section 3.3.

[38] These quantities are summarized in the following state vector:

$$\mathbf{x} = (k_1, \dots, k_n, q_1, \dots, q_r, A_1, \dots, A_s)^T. \quad (17)$$

[39] Only the lowermost 5.25 km of the aerosol extinction profile are represented in the state vector, while the aerosol extinction at higher altitudes, where the sensitivity of the measurement to aerosol extinction is low, is fixed in the forward model. Potential errors caused by this simplification are discussed in section 4.8.

[40] In the following, the potential of MAX-DOAS measurements to retrieve aerosol properties is investigated by simulating measurements using the SCIATRAN model described in section 3, which then serve as input for the inverse model based on equation (9). Measurement errors have been simulated by adding normally distributed random noise with a standard deviation of 5×10^{-4} to both the DOD and the intensity index, a noise level that is typically achieved by DOAS instruments [see, e.g., *Ferlemann et al., 2000; Frieb et al., 2001, 2004*]. The covariance matrix for the measurement noise, \mathbf{S}_e , is chosen to be diagonal, which means that the individual measurement errors are assumed to be independent.

[41] Unless stated otherwise, an a priori aerosol extinction profile which is linearly decreasing from 0.158 km^{-1} at the surface (corresponding to a visibility of 25 km) to 0.013 km^{-1} at an altitude of 3.5 km is used. The extinction profile above 3.5 km has been set to a standard free tropospheric and stratospheric profile adapted from the LOWTRAN library [*Kneizys et al., 1988*]. The variance σ_a of the a priori profile has been set to 100% of the a priori extinction at all levels, and a correlation of the aerosol extinction at different altitudes has been introduced by setting the a priori covariance for the extinction profile to

$$\mathbf{S}_{aj} = \sigma_{a_i}^2 \exp\left(-\frac{|z_i - z_j|}{\eta}\right). \quad (18)$$

[42] The correlation length η provides a constraint on the smoothness of the retrieval [*Barret et al., 2002*] and has been set to 0.5 km. For the spectral albedo, the average and covariance from representative surface types (different types of forest, grassland, urban) as provided by the MODTRAN database [*Berk et al., 1989*] has been used as a priori.

4.3. Aerosol Extinction Profile Retrieval

[43] The sensitivity of MAX-DOAS measurements to perturbations of the aerosol extinction at different altitudes is quantified by the weighting functions. Examples for typical weighting functions, calculated for an SZA of 85° , an azimuth angle of 90° and the smooth a priori aerosol extinction profile with a visibility of 25 km described in section 4.2, are shown in Figure 6. The weighting functions are expressed in dimensionless units by calculating the

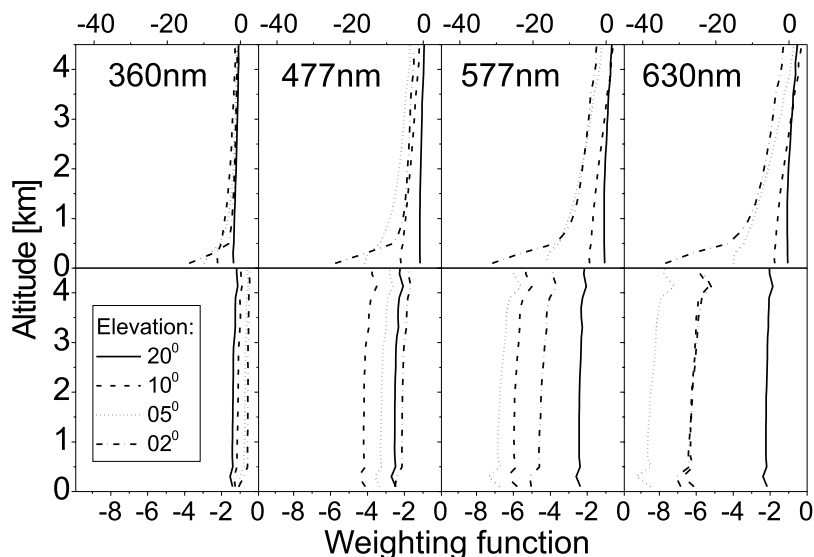


Figure 6. Weighting functions for (top) the O₄ optical depth and (bottom) the intensity index at four O₄ absorption bands centered around 360, 477, 577, and 630 nm. For further details, see text.

partial derivatives of the O₄ DOD, $\partial\Delta\tau(\lambda, \alpha)/\partial\Delta\tau_A(z)$, and the intensity index, $\partial\tilde{I}(\lambda, \alpha)/\partial\Delta\tau_A(z)$, with respect to the partial AOD $\Delta\tau_A(z) = k(z)\Delta z$ in the layer at altitude z and with a vertical extension Δz . For better comparison, the O₄ weighting functions are normalized by the vertical optical depth of O₄ at the respective wavelength. Note that the weighting functions shown here will vary with the extinction profile owing to the nonlinear nature of the problem.

[44] As expected, the weighting functions of the O₄ DOD are characterized by a strong peak at the surface and a rapid decrease with altitude, indicating a high sensitivity to aerosols near the ground. The sensitivity for aerosols near the surface is highest at small elevation angles owing to the longer light paths through the lowermost atmospheric layers. Measurements of the O₄ DOD at the 577 and 630 nm absorption bands show the highest sensitivity to aerosols owing to the higher transparency of the atmosphere at larger wavelengths.

[45] In contrast to O₄, the weighting functions for the intensity index are almost constant as a function of altitude, which means that measurements of the relative intensity do not yield any information on the altitude distribution of aerosols (note that this is not always the case as it is a result of the weighting function being calculated for a smooth aerosol extinction profile). However, measurements of the intensity index provide a strong constraint for the AOD and for aerosol optical properties, which will be shown later. The intensity weighting functions are generally negative owing to the stronger enhancement in intensity for the zenith compared to the off-axis viewing with increasing aerosol load.

[46] To investigate the capability of MAX-DOAS measurements to retrieve aerosol extinction profiles, four retrievals based on synthetic measurements using different sets of input data have been performed: (retrieval A) the O₄ DOD at 477 nm only, (retrieval B) the O₄ DOD at four absorption bands (360, 477, 577 and 630 nm), (retrieval C) the O₄ DOD and intensity index at 477 nm only, and (retrieval D) the O₄ DOD and intensity index at 360, 477,

577 and 630 nm. All retrievals are based on simulated measurements at four off-axis directions of 20°, 10°, 5° and 2° elevation, a solar zenith angle of 85° and an azimuth angle of 90°. A zenith sky spectrum at the same solar zenith angle serves as reference. Both the a priori and the true aerosol extinction profile have been set to the standard a priori profile with 25 km visibility as described previously.

[47] The averaging kernels of the aerosol extinction profiles for these retrievals are shown in Figures 7a–7d, respectively. Also shown are the areas (Figure 7e) and spread functions (Figure 7f) of the averaging kernels. Note that the spread as defined in equation (15) gives no meaningful estimate of the vertical resolution at the surface. This is caused by the negative lobes of the surface averaging kernels at higher altitudes discussed below.

[48] The averaging kernels for retrieval A show a distinct peak for the lowermost two layers centered around 100 and 300 m only, while the averaging kernels at higher altitudes are very broad and are centered around 1 km, rather than at their nominal altitudes. Thus only information on the aerosol extinction below 500 m can be derived when using merely the O₄ DOD at a single wavelength. The information on aerosols at higher altitudes is strongly improved when including measurements at four O₄ absorption bands in the measurement vector in retrieval B. The averaging kernels are now separated also at altitudes above 500 m, peak closer to their nominal altitudes, and are less broad than in retrieval A. Furthermore, the vertical resolution and the sensitivity of the retrieved to the true aerosol extinction near the surface have improved. A similar sensitivity for the aerosol extinction at high altitudes as in retrieval B can be achieved when using the DOD of O₄ and the intensity index at a single wavelength for the aerosol profile retrieval, as shown in Figure 7c. However, the vertical resolution at the lowermost two layers is slightly reduced compared to retrieval B. Finally, using the O₄ DOD plus the intensity index measured at four absorption bands yields the averaging kernels shown in Figure 7d. In this case, the averaging kernels within the lowermost 2 km peak at about their nominal

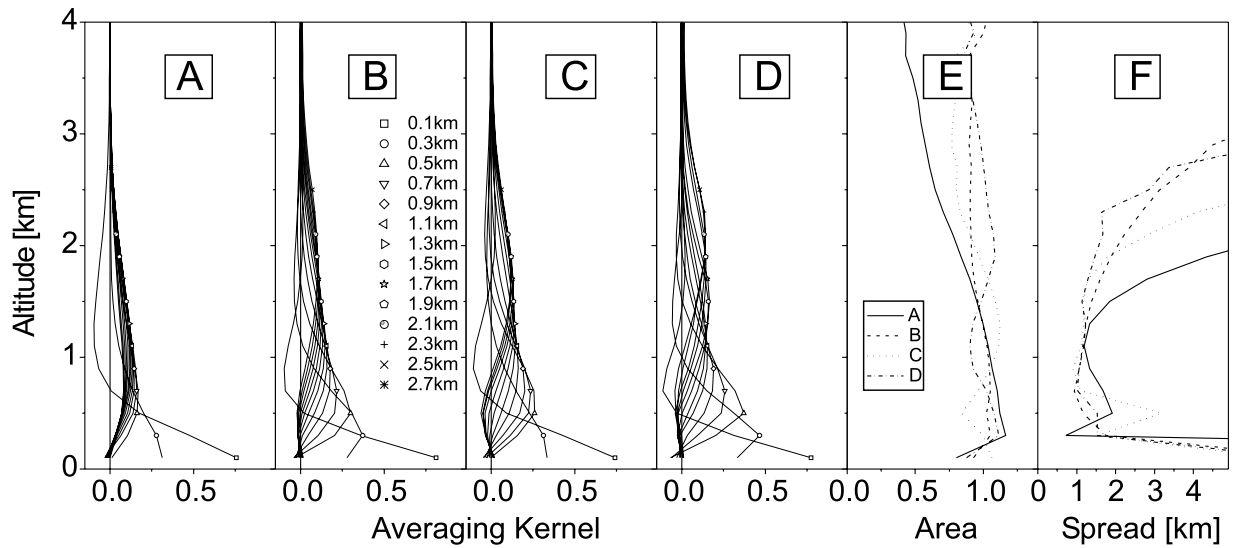


Figure 7. (a–d) Averaging kernels for the aerosol extinction profile retrievals A to D (for further details, see the text). Also shown are the corresponding averaging kernel (e) areas and (f) spreads.

altitudes, and the vertical resolution ranges from ≈ 300 m at the surface (estimated from the FWHM rather than from the spread function) to ≈ 1.5 km at 2 km altitude. A general feature all aerosol retrievals have in common is a negative lobe of the surface averaging kernel at higher altitudes, which implies that an increase in aerosol extinction around 1 km causes a decrease in sensitivity near the surface.

[49] The averaging kernel areas of retrievals B to D shown in Figure 7e are close to unity at all altitudes. Thus most information comes from the measurements rather than from the a priori except for retrieval A, where this is only the case below altitudes of ≈ 1.5 km.

[50] The error components of the aerosol extinction profile retrievals A to D are shown in Figure 8. The a priori error (set to 100% of the a priori extinction at all levels) is shown as a solid line. The retrieval error (dashed line) is

largely dominated by the smoothing error (dotted line). The retrieval noise (dash-dotted line) is much smaller in all cases. This implies that the information content of MAX-DOAS measurements is the limiting factor for the accuracy of the aerosol profile retrieval, while the random error in measured O₄ optical depths and intensities plays only a minor role. The retrieval error for the surface extinction is similar for all four retrievals with a value of ≈ 0.04 km⁻¹, corresponding to an error in visibility of about 6 km for this scenario that is based on a relatively clear atmosphere with a visibility of 25 km. Using only the O₄ DOD from a single absorption band (retrieval A), the retrieval error has values close to the a priori error above about 2 km, which indicates that the measurement is not sensitive to aerosols at these altitudes. In contrast, the retrievals including the intensity index and/or the O₄ DOD at several wavelengths (retrievals

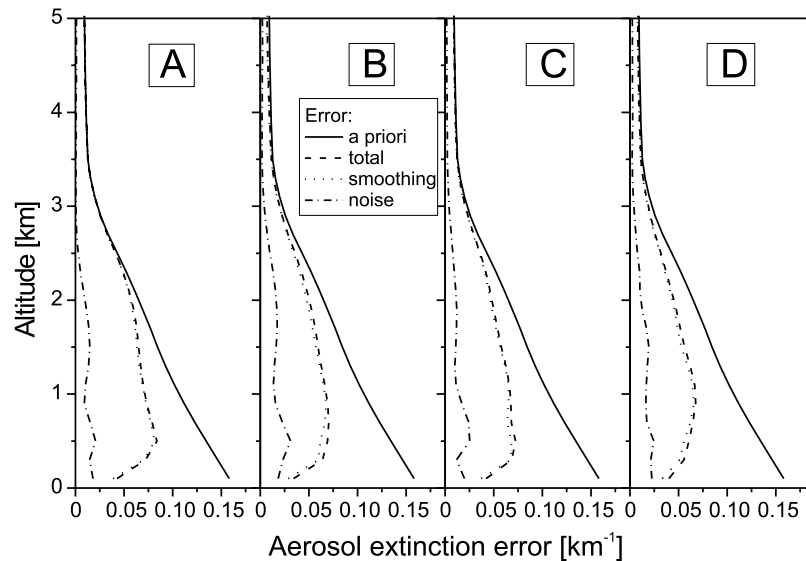


Figure 8. Error components of the aerosol extinction profile retrievals A to D. For further details, see text.

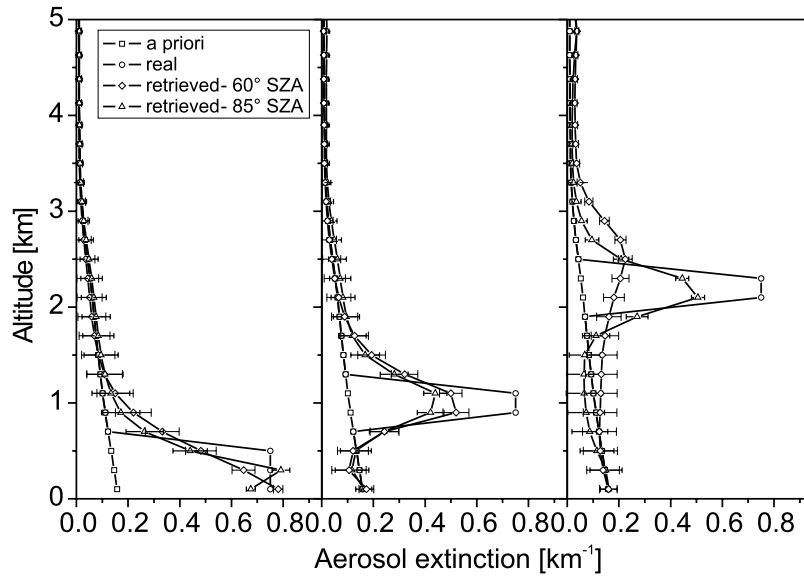


Figure 9. Examples for the aerosol extinction profile retrieval for a layer of strongly enhanced aerosols (left) at the surface and around (middle) 1 km and (right) 2.1 km. A priori and true profiles are indicated by squares and circles, and retrieved profiles for SZAs of 60° and 85° are diamonds and triangles, respectively. The error bars indicate the retrieval error. For more details, see text.

B to D) yield a retrieval error which is significantly smaller than the a priori error up to altitudes of about 3 km. As expected, the smallest retrieval errors are found for retrieval D with a combination of O₄ and intensity measurements at four wavelengths. In this case, the retrieval error remains below 0.068 km⁻¹ at all altitudes.

[51] Examples for the aerosol extinction profile retrieval for layers of strongly enhanced aerosols present at different altitudes are shown in Figure 9. The retrievals are performed at SZAs of 60° and 85° using retrieval scheme D. An enhanced layer of aerosols with an extinction coefficient of 0.75 km⁻¹ (corresponding to a visibility of 5.2 km) from the surface up to an altitude of 500 m is very well reproduced by the retrieval (Figure 9, left), both in terms of the absolute values of the extinction and the vertical extent. A very small error in surface extinction of only ≈ 0.018 km⁻¹ is achieved both for the retrieval at 60° and 85° SZA. A layer of enhanced aerosols at 1 km is also reproduced by the retrievals (Figure 9, middle), although the retrieved profiles are smoothed as a result of the limited vertical resolution of the measurements. The retrieval at 60° SZA yields slightly better results (less smoothing) than at 85° SZA. An aerosol enhancement at 2.1 km (Figure 9, right) is well reproduced at 85° SZA, both regarding vertical extent and center altitude. The retrieval at 60° SZA is not able to reproduce this layer realistically, the retrieval profile is strongly smoothed and peaks above the true aerosol layer.

[52] The reason for the sensitivity of MAX-DOAS measurements during twilight to aerosol enhancements even at high altitudes is the response of the weighting functions to such a disturbance of the profile, as shown for the enhancement at 2.1 km in Figure 10. In contrast to the weighting functions of a smooth profile (see Figure 6), both the O₄ (Figure 10, left) and the intensity (Figure 10, middle)

weighting functions show a strong peak at altitudes where the aerosol enhancement is present, reflecting the strong nonlinear nature of the problem. As a result, the averaging kernels for the layers at 2.3 and 2.5 km show a pronounced peak at their nominal altitudes, indicating that the retrieval is sensitive to the true profile altitudes where an enhancement in aerosols is present.

4.4. Kalman Smoothing

[53] Finding an appropriate a priori for an aerosol retrieval is not trivial, and using inappropriate a priori constraints can easily cause unrealistic or strongly biased results. Sources of a priori information can be a climatology, colocated measurements by other instruments such as LIDAR profiles, the AOD from satellite borne radiometers, the aerosol distribution determined by numerical models, or simply estimates of the meteorological visibility from visual observations.

[54] However, the result of the retrieval should preferably be independent from measurements by other instruments. If measurements are performed sequentially in time, this can be achieved by using the retrieved state vector $\hat{\mathbf{x}}_{k-1}$ from the previous measurement at time t_{k-1} to determine an estimate for the a priori $\mathbf{x}_{a,k}$ at time t_k , a technique that is referred to as Kalman filtering [Kalman, 1960]. This method is very similar to the widely used technique of data assimilation in numerical models. It requires a dynamic model $\mathbf{M}^\dagger \equiv \mathbf{M}^\dagger(\mathbf{x}(t_{k-1}), \mathbf{x}(t_k))$ (the arrow indicates that the model operates forward in time), which is able to predict the state of the atmosphere $\hat{\mathbf{x}}_k^\dagger$ at time t_k given the state at a previous time t_{k-1} .

[55] In case of the reprocessing of data, measurements in the future are also available, and Kalman filtering can also be performed backward in time based on an operator \mathbf{M}^\downarrow which predicts the state $\hat{\mathbf{x}}_k^\downarrow$ at t_k based on a future state $\hat{\mathbf{x}}_{k+1}^\downarrow$

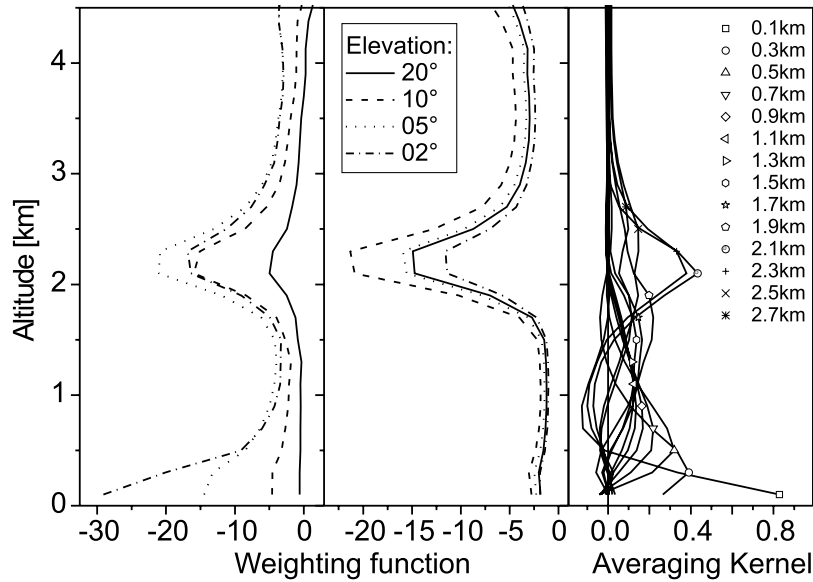


Figure 10. Weighting functions for (left) the O₄ differential optical depth, (middle) the intensity index, and (right) averaging kernels for a retrieval at 85° SZA with an enhanced aerosol layer at 2.1 km (triangles in the right panel of Figure 9). The weighting functions are shown for a wavelength of 577 nm.

at time t_{k+1} . Forward and backward estimates are combined in an optimal way using

$$\hat{\mathbf{S}}_k = \left(\hat{\mathbf{S}}_{a_k}^{\uparrow-1} + \hat{\mathbf{S}}_k^{\downarrow-1} \right)^{-1} \quad (19)$$

$$\hat{\mathbf{x}}_k = \hat{\mathbf{S}}_k \left(\hat{\mathbf{S}}_{a_k}^{\uparrow-1} \hat{\mathbf{x}}_{a_k}^{\uparrow} + \hat{\mathbf{S}}_k^{\downarrow-1} \hat{\mathbf{x}}_k^{\downarrow} \right), \quad (20)$$

which yields the so-called Kalman smoothed estimate $\hat{\mathbf{x}}_k$ at time t_k .

[56] Here a Kalman smoother is applied to MAX-DOAS measurements of aerosols using a linear dynamic model based on simple assumptions of the temporal variability of the atmosphere. Given an estimate of the state vector at time t , it can be expected that a similar state is present at time $t \pm \Delta t$ if the time span Δt is not much larger than a characteristic time τ which quantifies the timescale on which the state of the atmosphere varies. However, the estimate of the state vector at time t will contain only little information on the atmospheric state at times $t \pm \Delta t$ if $\Delta t \gg \tau$, which means that the predicted state and its covariance should converge to the climatological mean for large Δt . The Kalman filter used here is based on the following relaxation model:

$$\mathbf{x}_{a_k} = \hat{\mathbf{x}}_{k\pm 1} e^{-\frac{\Delta t}{\tau}} + \mathbf{x}_a \left(1 - e^{-\frac{\Delta t}{\tau}} \right) \quad (21)$$

$$\mathbf{S}_{a_k} = \hat{\mathbf{S}}_{k\pm 1} e^{-2\frac{\Delta t}{\tau}} + \mathbf{S}_a \left(1 - e^{-2\frac{\Delta t}{\tau}} \right), \quad (22)$$

with $\Delta t = |t_k - t_{k\pm 1}|$. The dynamical models for forward and backward prediction are the same, and \mathbf{x}_a and \mathbf{S}_a are fixed quantities representing the climatological mean and variability, respectively, of the state vector. Here τ quantifies the timescale of the temporal variability of the state vector and

provides a constraint for the smoothness of the aerosol profile in time.

[57] The Kalman smoother (21, 22) has been applied to the simulated diurnal variation of MAX-DOAS measurements at equinox and 50° latitude. Measurements at 20°, 10°, 5°, and 2° elevation relative to a zenith sky reference have been simulated for the afternoon (1200–1815 local time). Measurements of a set of elevation angles have been assumed to be performed in 15-min intervals. The timescale for the temporal variability of the aerosol extinction has been set to $\tau = 1$ hour. The true profile at noon has been set to the standard aerosol extinction profile (25 km visibility, linear decrease of aerosol extinction with altitude), which also serves as the initial a priori for both the forward and backward filter. The aerosol extinction has been gradually increased with time by scaling the profile in the lowermost 3 km by a constant factor up to a rather extreme value of 0.7 km⁻¹ for the surface extinction (corresponding to a visibility of 5.6 km) at 1800 local time as shown by the dashed lines in Figure 11. Using the simulated measurements for this scenario, retrievals were performed using the O₄ DODs at 477 nm only (Figures 11a and 11b) and the full measurement vectors with O₄ DODs and the intensity indices at four absorption bands (360, 477, 577 and 630 nm) (Figures 11c and 11d).

[58] In a first model run, retrievals were performed without Kalman smoother and using a fixed standard 25 km a priori extinction profile (Figures 11a and 11c). In this case, the true profiles (open symbols) are poorly reproduced by the retrieval (solid symbols). Owing to the high aerosol abundances occurring later in the day, the measurements are not compatible with the constraints given by the fixed a priori state vector and unrealistic retrieval results are produced. In particular, the lack of sensitivity to the aerosols at high altitudes for a retrieval using the O₄ DODs at a single absorption band (Figure 11a) causes an underestimation of the extinction above about 1 km,

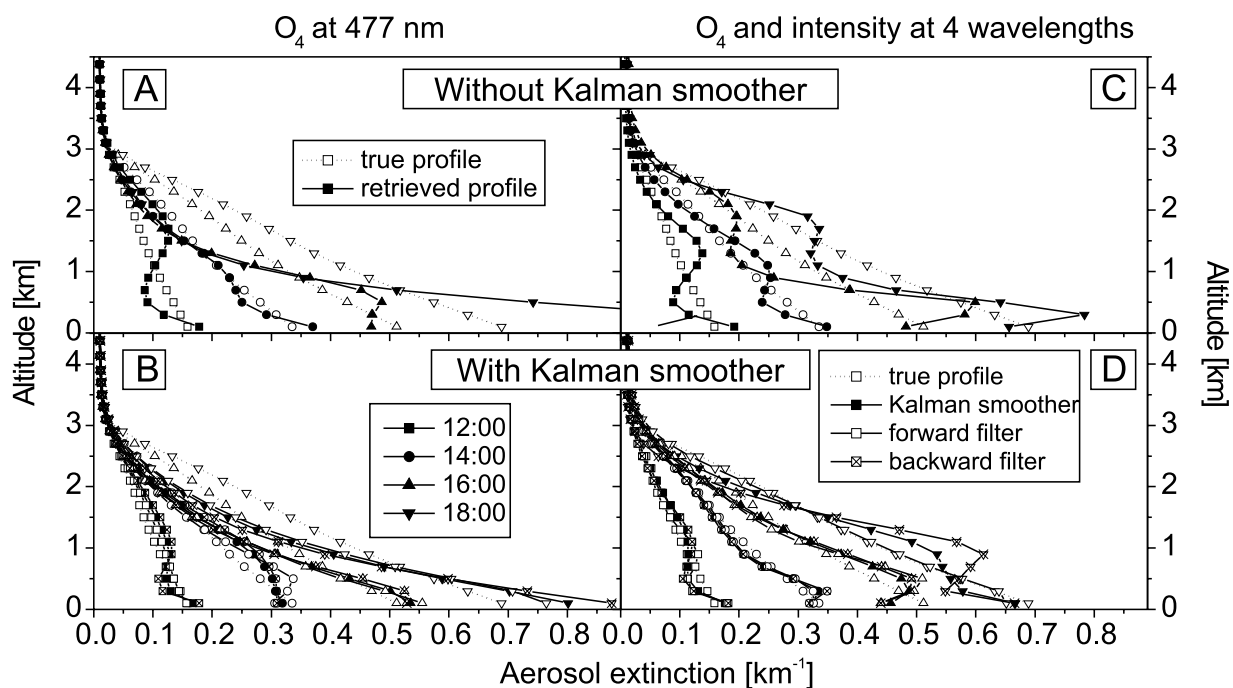


Figure 11. Simulated retrieval of the diurnal variation of the aerosol extinction profile for a gradually increasing linear profile. (a, b) Measurement vector containing the O₄ DODs at 477 nm; (c, d) measurement vector contains the O₄ DODs and intensity indices at 360, 477, 577, and 630 nm. Figures 11a and 11c have no Kalman smoothing, and are fixed a priori with 25 km visibility; Figures 11b and 11d use a Kalman smoother as described in the text. Profiles estimated by the forward (open symbols), backward (crossed symbols), and combined (solid symbols) estimates are shown for every second hour only, while the measurements were simulated in 15-min intervals.

which is compensated by an overestimation near the surface. Strong oscillations around the true aerosol extinction profile occur in case of a retrieval with the full state vector (Figure 11c).

[59] Performing the retrievals with a Kalman smoother (Figures 11b and 11d) yields a strongly improved agreement between the true (small open symbols and dashed lines) and retrieved (solid symbols) aerosol extinction profiles. The retrieved aerosol extinctions at the surface agree well with the true values, although an overestimation (compensated by an underestimation at higher altitudes) occurs for high aerosol loads in case of the retrieval with O₄ DOD at a single wavelength (Figure 11b). This is a result of the low sensitivity of the O₄ DOD to aerosols at higher altitudes. The best results are achieved when applying the Kalman smoother to the full measurement vectors (Figure 11d). The oscillations occurring when using a fixed a priori are strongly reduced and the retrieved aerosol extinction profiles are in very good agreement with the true profiles.

[60] Also shown in Figures 11b and 11d are the forward and backward filtered estimates of the aerosol extinction profiles (open and crossed symbols, respectively). The forward filter starts with an initial a priori equal to the true extinction profile ($\mathbf{x} = \mathbf{x}_a$), whereas the backward filter starts with the same a priori but a 5 times higher aerosol load ($\mathbf{x} = 5 \times \mathbf{x}_a$). The backward filtered estimate shows an agreement with the true profile similar to the forward estimate already at 1600 local time (i.e., after seven time steps of 15 min each). This illustrates that convergence toward the true

profile is quickly achieved even if the true state vector strongly differs from the initial a priori estimate.

[61] From these sensitivity studies, it can be concluded that the technique of Kalman smoothing allows the retrieval of aerosol properties even under highly variable conditions, which is not possible using a fixed a priori extinction profile for each retrieval. Kalman smoothing is a computationally expensive procedure since it requires two retrievals for each measurement to be performed, one for the forward and one for the backward filter. However, applying a Kalman filter in forward direction only has been found to be sufficient in most cases.

4.5. Retrieval of the Aerosol Optical Depth

[62] To investigate the accuracy of the retrieval of the AOD, the total aerosol optical depth $\tau_A = \sum_i k_i \Delta z_i$ has been calculated from the Kalman smoothed extinction profiles of the scenario described in section 4.4 (gradually increasing aerosol load in the lowermost 3 km). The retrieved AOD as a function of the true AOD for three different model runs is shown in Figure 12.

[63] For the first model run (squares), only the O₄ DODs at a single wavelength of 477 nm are included in the measurement vector. In this case, the retrieved AODs are in fairly good agreement with the true values up to an AOD of 0.7, but a significant underestimation occurs for higher aerosol loads. The reason for this underestimation is that the Kalman smoother is not able to adapt the state vector to the rapid change in aerosol load owing to the limited information content of O₄ measurements at a single wavelength.

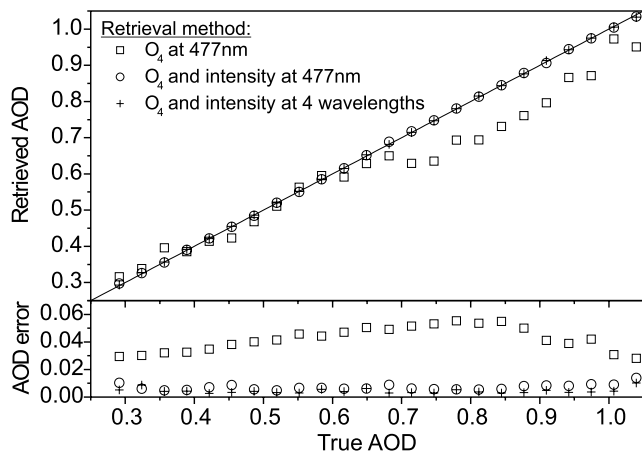


Figure 12. (top) Retrieved AOD as a function of true AOD for scenario I using three different sets of input data for the retrieval (for more details, see text). The solid line indicates the function $y = x$. (bottom) Corresponding retrieval errors.

The retrieval errors for this model run are in the order of 0.05 (see Figure 12, bottom).

[64] The precision of the AOD retrieval is strongly improved when including the intensity index in the measurement vector, with similar results when using only measurements at 477 nm (circles) and measurements at four O₄ absorption bands (pluses). Retrieved and true values are in very good agreement and the error in retrieved AOD remains below 0.01.

[65] It can be concluded that measurements of the O₄ DOD alone can already provide a reasonable estimate of the AOD. A precision comparable with measurements from sky radiometers can theoretically be achieved if the intensity index is considered in the retrieval in addition to the O₄ DOD. However, only random errors have been considered so far, but systematic errors will also contribute to the accuracy of the retrieved AOD. The impact of systematic errors on the AOD retrieval will be discussed in section 4.8.

4.6. Retrieval of Aerosol Optical and Microphysical Properties

[66] It has been shown in section 3.2 that MAX-DOAS measurements at different elevations and azimuth angles are sensitive not only to the aerosol extinction but also to optical and microphysical properties of aerosols. In particular, the variation of the intensity as a function of azimuth angle contains significant information on the phase function and single scattering albedo. A full retrieval of the latter two quantities, or alternatively the retrieval of the aerosol size distribution and complex refractive index, is not yet implemented in the retrieval algorithm. However, it will be shown in the following that information on aerosol optical properties can be obtained by retrieving the composition of different types of aerosol particles.

[67] Sensitivity study (I) focuses on the ability of MAX-DOAS measurements to distinguish between highly reflective and strongly absorbing aerosols by modeling a mixture of water-soluble aerosols and soot particles, with q being the fraction of soot aerosols in the mixture. The simulations have been performed under the assumption of a vertically

homogeneous aerosol composition. Simulated measurements of the O₄ DOD and intensity index have been calculated at an SZA of 60° using a fixed aerosol extinction profile with 25 km visibility and a varying soot fraction q . The aerosol extinction profile and the parameter q have been retrieved simultaneously using our inverse model. The a priori soot fraction has been set to $q_a = 0.5$ with an error of 0.5, and all retrievals were performed with a measurement vector consisting of the O₄ DOD and the intensity index. Four different model runs were performed, and the results are shown in Figure 13.

[68] In model run a, measurements at four elevation angles (20°, 10°, 5°, 2°) and a single azimuth angle of $\phi = 90^\circ$ were simulated using the O₄ DOD and intensity index at a single wavelength of 477 nm. In this case, a high error in retrieved soot fraction (squares in Figure 13) of more than 100% occurs for low abundances of absorbing aerosols ($q < 0.3$), but the error decreases with increasing q and drops below 0.1 for soot fractions higher than 0.5.

[69] The precision of the retrieval of soot fraction is slightly improved in model run b (circles) by using the same observation geometry as in run a (variation of the elevation angle only), but based on measurements at four O₄ absorption bands (360, 477, 577 and 630 nm). This is because intensity and O₄ absorption at different wavelengths contains implicit information on the wavelength dependence of the aerosol phase function, which allows a better distinction between absorbing and reflecting aerosols.

[70] Model runs c and d (triangles and pluses) are similar to runs a and b, respectively, but in this case, additional measurements at different azimuth angles have been modeled using the same set of 28 azimuth angles in the solar almucantar as for the measurements by sky radiometers within the AERONET network [Dubovik *et al.*, 2000; Dubovik and King, 2000] (2°, 2.5°, 3°, 3.5°, 4°, 5°, 6°, 10°, 12°, 14°, 16°, 18°, 20°, 25°, 30°, 35°, 40°, 45°, 50°, 60°, 70°, 80°, 90°, 100°, 120°, 140°, 160° and 180°). Owing to the variation in scattering angle by measuring at different azimuth angles, a good agreement between retrieved and true soot fraction is achieved. The retrieval errors for q

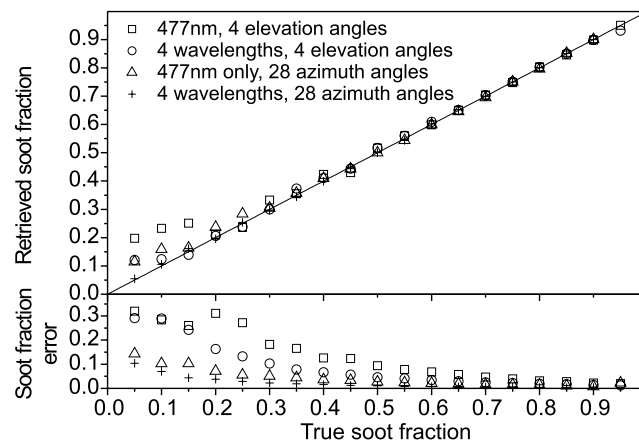


Figure 13. (top) Retrieved soot fraction q as a function of true soot fraction using four different sets of input data for the retrieval (for more details, see text). The solid line indicates the function $y = x$. (bottom) Corresponding retrieval errors.

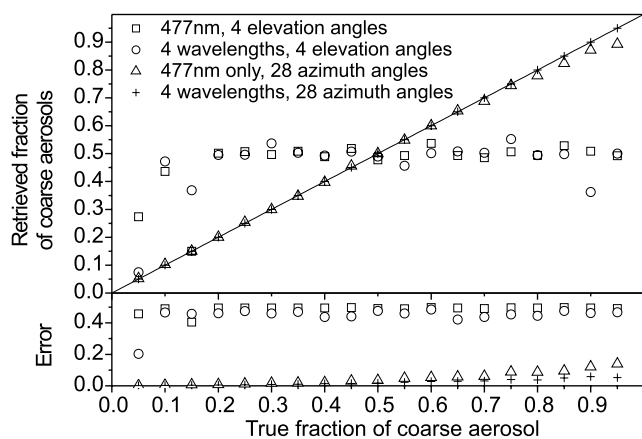


Figure 14. (top) Retrieved fraction of coarse mineral aerosols q as a function of the true values using four different sets of input data for the retrieval (for more details, see text). The solid line indicates the function $y = x$. (bottom) Corresponding retrieval errors.

remain below 0.1 in case of measurements at four wavelengths (run d), and are almost negligible (<0.03 for $q > 0.5$) both for runs c and d at high abundances of absorbing aerosols.

[71] Sensitivity study II focuses on the retrieval of the aerosol size distribution. The same model runs a to d as for sensitivity study I have been performed, but this time using a mixture of fine and coarse mineral aerosols with average radii of $0.07 \mu\text{m}$ (nucleation mode) and $1.9 \mu\text{m}$ (coarse mode), respectively. Both types of aerosols have identical refractive indices; q now quantifies the fraction of coarse aerosols. The results of this sensitivity study are shown in Figure 14. Model runs a and b yield retrieval errors for q equal to the a priori standard deviation of 0.5, which means that measurements at different elevation angles do not contain any significant information on the size distribution of aerosols. However, a scan at different azimuth angles (runs c and d) allows the size distribution to be determined with a very high precision. Retrieved and true values for q are in very good agreement, and the retrieval error is smaller than 0.06 if measurements at four O₄ absorption bands are considered (run d). The best sensitivity for the size distribution is achieved if small particles dominate ($q < 0.5$) with an error in q of less than 0.03.

[72] The optical and microphysical properties of aerosols are still represented in a simplified way in the retrieval algorithm. However, the sensitivity studies presented here suggest that significant information on aerosol optical properties can be derived from MAX-DOAS measurements, and a full retrieval of the aerosol size distribution and refractive index should be possible in a similar way as for the measurements from sky radiometers.

4.7. Information Content of MAX-DOAS Aerosol Measurements

[73] On the basis of the examples in section 4.3, it has been shown that the sensitivity of the retrieval of aerosol properties from MAX-DOAS measurements depends on the aerosol extinction profile itself as a result of the nonlinear nature of the problem. In this section, the dependency of the

information content of aerosol extinction profile retrievals on the atmospheric conditions and viewing geometry is investigated more systematically by performing aerosol extinction profile retrievals at varying AOD, SZA and relative azimuth angle.

[74] The dependency of the information content on AOD has been investigated by setting the true aerosol extinction profile linearly decreasing with altitude from the surface up to 3 km, and the profile has been scaled in the lowermost 3 km to AODs between 0 and 5. The a priori has been set equal to the true profile ($\mathbf{x} = \mathbf{x}_a$), and measurements at four elevation angles (20° , 10° , 5° and 2°) relative to a zenith sky spectrum have been included in the measurement vector. Quantities specifying retrieval errors, information content and vertical resolution have been determined on the basis of retrievals using the O₄ DOD only and using both the O₄ DOD and the intensity index as shown in the left and right panels of Figure 15, respectively. Results are shown for retrievals using simulated measurements at a single O₄ absorption line only (thin lines), and for retrievals based on simultaneous measurements at 360, 477, 577 and 630 nm (thick gray lines).

[75] For retrievals using only a single O₄ absorption line, the best results are achieved at 577 nm (dotted lines) and worst at 360 nm (solid lines). Optimal vertical resolution is obtained at large wavelengths for two reasons: (1) higher transparency of the atmosphere and therefore better geometrical enhancements and (2) largest cross section at 577 nm, which yields a better signal to noise ratio. As expected, the best results are achieved using the combined retrieval at four wavelengths (thick gray lines). In general, the performance of the retrieval is not very good in a clear atmosphere ($\tau_A < 0.2$). Under these conditions, large errors in surface aerosol extinction and AOD occur and the vertical resolution of the retrieved profile is poor.

[76] Regarding error in surface aerosol extinction, the variation of visibility with wavelength leads to different minima in surface aerosol extinction error depending on the absorption band used for the retrieval: The best estimate for the surface aerosol extinction occurs at an AOD of ≈ 0.35 (error of $\approx 30\%$) for the 360 nm absorption band, and at an AOD of ≈ 0.95 (error of $\approx 16\%$) for the 577-nm absorption band. The surface aerosol extinction error is less than 20% over a wide range of atmospheric conditions ($0.35 < \tau_A < 2.5$) for the combined retrieval at four wavelengths. Including the intensity index in the retrieval only leads to small reductions in surface aerosol extinction error, confirming that the sensitivity of the intensity index to the vertical profile is small in the case of a smooth (linearly decreasing) aerosol extinction profile.

[77] Regarding error in AOD, using only the O₄ DOD as input for the retrieval, the AOD cannot be determined with a precision better than 5% and the error in AOD quickly increases with increasing aerosol load. The AOD is estimated much better if the intensity index is included, in particular when using measurements at 577 or 630 nm, or for the retrieval using four wavelengths: The error in AOD remains below 4% in all cases and is even below 1% over a wide range of conditions ($0.13 < \tau_A < 2.3$) for the retrieval at four wavelengths. However, the error in AOD is still very high for the retrieval at short wavelengths (360 and 477 nm) even when including the intensity index, in particular at

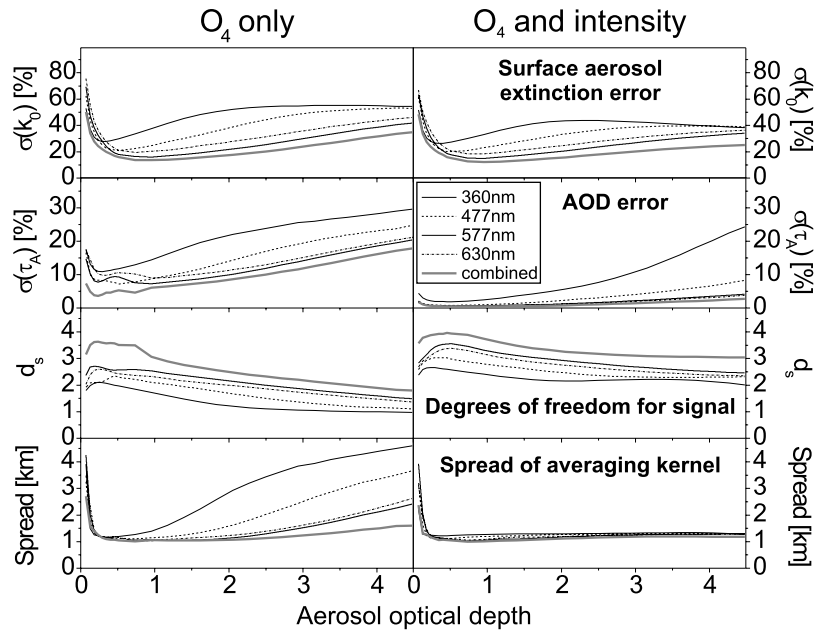


Figure 15. Parameters quantifying the information content of MAX-DOAS measurements for aerosol extinction profile retrievals as a function of aerosol optical depth. (top to bottom) Relative error in surface aerosol extinction, relative error in AOD, degrees of freedom for signal, and spread of averaging kernel at 1.1 km altitude (left) using the O₄ DOD only and (right) using the O₄ DOD and intensity index. Thin lines denote retrievals using only a single O₄ absorption band at the wavelengths denoted in the legend; thick gray lines denote retrieval using simultaneous measurements at four O₄ absorption bands (360, 477, 577, and 630 nm).

high AODs. These findings again confirm that the O₄ DOD contains information mainly on the shape of the aerosol extinction profile, while the intensity index provides a strong constraint for the AOD.

[78] The information content is shown in Figure 15 in terms of the degrees of freedom for signal d_s (equation (14)), which determines the number of independent pieces of information contained in the measurements. For the retrieval at four wavelengths, d_s has a relatively broad maximum for AODs around 0.5 with values reaching about 3.5 and 4 for the retrievals without and with intensity index, respectively. The corresponding measurement vectors contain 16 and 32 elements (4 elevation angles times 4 wavelengths), respectively, which means that the measurements are far from independent. In particular, the intensity index only adds about 0.5 pieces of information to the aerosol profile retrieval.

[79] The vertical resolution of the retrieved aerosol extinction profile, as quantified by the spread at 1.1 km, is low in a very clear atmosphere ($\tau_A < 0.2$) where the spread can reach values of up to 4 km. However, an almost constant spread of about 1 km is achieved for $\tau_A > 0.25$ by combining measurements of the O₄ DOD at four wavelengths and/or by including the intensity index. In particular, the vertical resolution of the retrieval including the intensity index is about the same at all wavelengths and is not improved significantly when combining measurements from different O₄ absorption bands. The vertical resolution becomes poor at high aerosol load if only the O₄ DOD at a single absorption band is included in the retrieval.

[80] The information content of MAX-DOAS aerosol measurements as a function of SZA for a visibility of

25 km (all other parameters as for the calculations shown in Figure 15) is shown in Figure 16. The increase in spectral noise with SZA has been considered for these calculations by setting the measurement errors to the average RMS residual obtained from the analysis of three months of zenith sky DOAS measurements at Neumayer station in the wavelength interval between 490 and 555 nm (for details of the instrument see Frieß *et al.* [2004]). The degrees of freedom for signal remain almost constant up to an SZA of 90° and only decrease slightly at higher SZAs (from 4.5 to 4 in case of the combined O₄ DOD and intensity retrieval at four wavelengths). Except for the retrieval using the 360-nm O₄ absorption band, the error in AOD does not depend significantly on SZA, and the error in aerosol extinction at the surface increases only slightly during twilight.

[81] The information content of the aerosol retrieval as a function of relative azimuth angle at 85° SZA and for a visibility of 25 km is illustrated in Figure 17. No systematic dependency of the quality of the retrieval on azimuth angle is apparent if only the O₄ DOD is included in the retrieval (Figure 17, left). Retrievals using both the O₄ DOD and the intensity index (Figure 17, right) yield the best results at small azimuth angles ($\phi < 45^\circ$), both in terms of degrees of freedom for signal and error of aerosol extinction at the surface. The AOD can be retrieved equally good at all azimuth angles.

4.8. Systematic Errors

[82] So far, only random errors on the retrieval of aerosol properties by MAX-DOAS have been considered by adding random noise to the O₄ DODs and intensity indices and by using a corresponding measurement covariance matrix S_e .

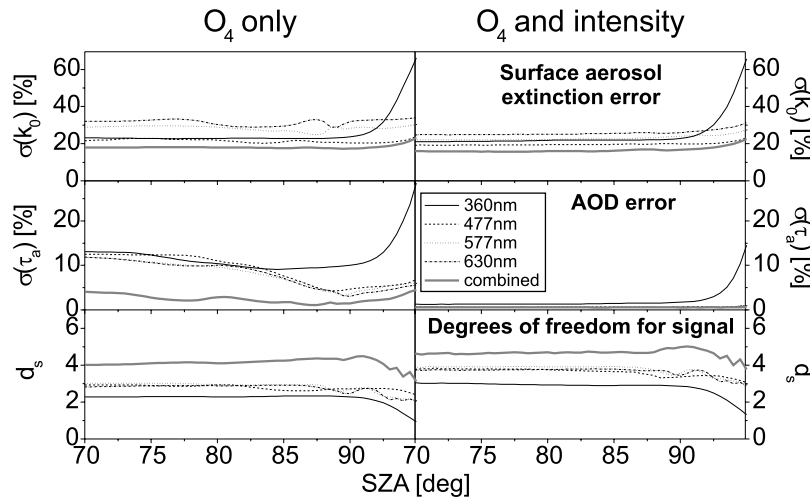


Figure 16. Parameters quantifying the information content of MAX-DOAS measurements for aerosol extinction profile retrievals as a function of solar zenith angle for a visibility of 25 km. (top to bottom) Relative error in surface aerosol extinction, relative error in AOD, and degrees of freedom for signal (left) using the O₄ DOD only and (right) using the O₄ DOD and intensity index. Thin lines denote retrievals using only a single O₄ absorption band at the wavelengths denoted in the legend; thick gray lines denote retrieval using simultaneous measurements at four O₄ absorption bands (360, 477, 577, and 630 nm).

However, numerous sources of systematic errors exist which have a potential impact on the precision of the aerosol retrieval.

[83] As discussed in section 4, the forward model $F(\mathbf{x}, \mathbf{b})$ depends both on the state vector \mathbf{x} , which is retrieved by the inverse model, and on model parameters \mathbf{b} which are kept fixed during the retrieval. Given that the true value of the model parameters is \mathbf{b} and the model parameters used in the retrieval are $\hat{\mathbf{b}}$, an uncertainty $\mathbf{b} - \hat{\mathbf{b}}$ in forward model parameters will lead to an error in the retrieved state vector. Model parameter errors have been quantified by simulating noise-free measurements using $\mathbf{y} = F(\mathbf{x}, \mathbf{b})$ and by performing a retrieval with \mathbf{y} as measurement vector, but with the model parameters set to $\hat{\mathbf{b}}$. The model parameter errors are then given by the difference between true and retrieved state vector, $\mathbf{x} - \hat{\mathbf{x}}$. In the following, model

parameter errors will be discussed for two scenarios with low and high aerosol load (25 km and 5 km visibility, respectively) and measurements at elevations of 20°, 10°, 5° and 2°. Both the O₄ DOD and the intensity index at four wavelengths (360, 477, 577 and 630 nm) have been considered in the retrieval. The resulting systematic errors for the aerosol extinction at the surface and for the AOD are summarized in Table 1.

[84] The aerosol extinction profile has been retrieved in the lowermost 5 km of the atmosphere only, while the aerosol profile in the upper troposphere and stratosphere has been kept fixed using typical extinction profiles for midlatitudes. The impact of incorrect estimates of these upper parts of the profile on the retrieval has been investigated by assuming that the aerosol extinction profile in the upper troposphere (5–11 km) and stratosphere (above 11 km) is

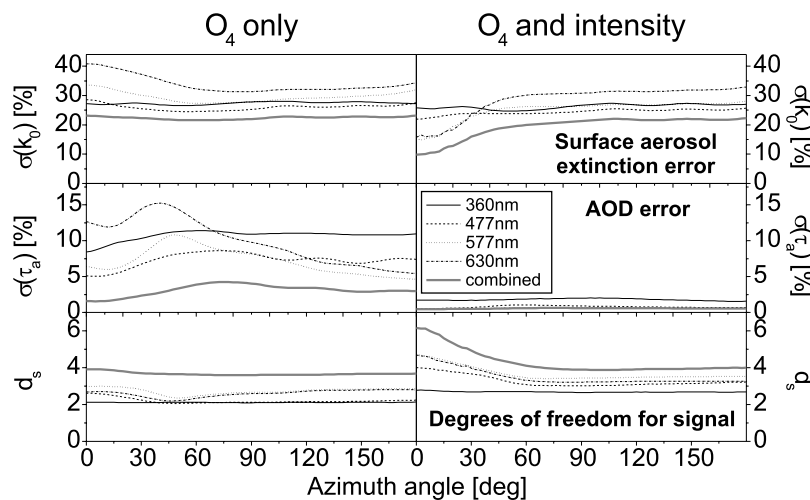


Figure 17. Parameters quantifying the information content of MAX-DOAS measurements for aerosol extinction profile retrievals as a function of azimuth angle.

Table 1. Summary of Systematic Errors of the Aerosol Extinction Profile Retrieval

Error Source	Test	25 km visibility		5 km visibility	
		Surface Extinction Error, %	AOD Error, %	Surface Extinction Error, %	AOD Error, %
Fixed profile in upper troposphere	doubling of extinction in upper troposphere	3.7	7.5	0.3	1.5
Fixed profile in stratosphere	doubling of extinction in stratosphere	4.0	1.5	0.3	0.05
Pointing error	error of 0.1° in elevation angle	10.9	0.5	1.9	0.2
Neglecting FOV	simulation of 1° FOV	3.6	0.1	0.04	0.02
Systematic error in O ₄ DOD	1% systematic error	3.0	0.3	1.5	0.01
Systematic error in intensity index	1% systematic error	0.4	1.6	0.5	1.4
Error in pressure profile	error of 10 hPa in surface pressure	3.7	1.0	2.7	0.2

underestimated by a factor of 2. For the low-aerosol scenario, this leads to an error of up to 4% in surface extinction and, in case of an incorrect aerosol extinction in the upper troposphere, to an error of 7.5% in AOD. However, the errors are much smaller for the high-aerosol scenario with a maximum error in AOD of 1.5%. These errors do not exhibit a principal restriction to the accuracy of the aerosol retrieval since the retrieval can be easily extended to higher altitudes (with higher computational effort) if the uncertainty in upper tropospheric or stratospheric aerosol load should be significant.

[85] To estimate the retrieval error caused by pointing inaccuracies, errors in elevation angle of 0.1° have been simulated under the assumption that the errors are independent for each viewing direction. This misalignment of the telescope causes an error of more than 10% in surface extinction for the low-aerosol case, and about 2% at high aerosol load, while the error in AOD is less than 1%. Thus a precise alignment of the MAX-DOAS telescope is essential. However, the pointing error is expected to be smaller in practice since the errors in viewing direction are usually not independent, but the alignment of the viewing directions relative to each other can be very precise, for example when using a stepper motor for the movement of the telescope. The main source of uncertainty is, in this case, a tilt of the whole entrance optics.

[86] The forward model simulates point-like measurements, while MAX-DOAS instruments usually have a field of view (FOV) in the order of 1°, and thus collect light from a range of elevation angles simultaneously. The error caused by this simplified assumption in the forward model has been investigated by simulating measurements with a FOV of 1°, but by assuming a point-like measurement in the retrieval. The resulting systematic errors are much smaller (3.6% in surface extinction in the low-aerosol case, otherwise below 0.1%) than the previously described errors caused by pointing inaccuracies because the contributions of light from above and below the center of the FOV partially compensate. However, an instrument with a FOV which is as small as possible is desirable to minimize this error source.

[87] Systematic errors in the O₄ DOD can be caused by uncertainties in the O₄ cross section and by systematic errors in the radiative transfer model. A systematic error of 1% in O₄ DOD leads to an uncertainty of 3% and 1.5% in surface extinction for the low- and high-aerosol scenarios,

respectively, while the impact on the retrieved AOD is negligible.

[88] The accuracy of the intensity index can be affected by instrumental stray light, nonlinearities of the detector and by inaccuracies in the radiative transfer model. An error in intensity index of 1% causes an error of about 1.5% in AOD, but has only a very small impact on the retrieved surface extinction (<0.5%).

[89] Variations in the atmospheric pressure profile affect the O₄ profile owing to its proportionality to the square of the O₂ concentration. Furthermore, changes in pressure have an impact on the light path distribution since Rayleigh scattering depends on the air density. The error caused by pressure variations has been investigated by assuming that the true surface pressure is 10 hPa higher than assumed in the retrieval. This leads to errors in retrieved surface extinction of 3.7% and 2.7%, and in AOD of 1% and 0.2% for the low- and high-aerosol scenarios, respectively.

[90] Examples for the error patterns introduced by systematic measurement errors, quantified by the difference between true and retrieved aerosol extinction profiles, are shown in Figure 18. Systematic overestimations of 1% in

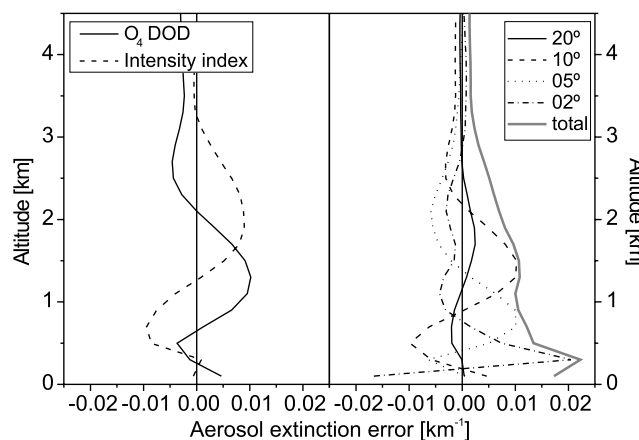


Figure 18. Error patterns (difference between true and retrieved aerosol extinction profiles) generated by (left) a systematic overestimation of the O₄ DODs and intensity indices of 1% and (right) an error of 0.1° in elevation angle. The thick gray line shows the total pointing error if the errors in elevation angle are independent for each viewing direction.

O₄ DODs and intensity indices cause oscillations of the retrieval around the true profile in the order of $\pm 0.01 \text{ km}^{-1}$ (Figure 18, left panel). The errors in the aerosol extinction profile caused by pointing inaccuracies of 0.1° shown in Figure 18 (right panel) illustrate that a precise pointing of the MAX-DOAS telescopes is essential to avoid strong systematic errors in the retrieval. A pointing inaccuracy of the measurement at 2° elevation angle causes an underestimation of the aerosol extinction at the surface of more than 0.015 km^{-1} and an overestimation of similar magnitude at 300 m altitude. As expected, the sensitivity of the retrieval to pointing errors decreases with increasing elevation angle owing to the decrease in the length of the light paths through the lowermost atmospheric layers. The total error in aerosol extinction in the lowermost 500 m is $\approx 0.02 \text{ km}^{-1}$ if the pointing errors at the different viewing directions are independent (thick gray line).

[91] Errors introduced by incorrect assumptions on the surface albedo have been investigated by performing retrievals with an a priori albedo $A_a = 0.5 \pm 0.1$. The true albedo A has been varied between 0.05 and 0.95. The results of these calculations, performed using the O₄ optical depth and intensity index, are shown in Figure 19 for the O₄ absorption bands at 360, 477, 577 and 630 nm. The retrieved aerosol extinction at the surface is in agreement with the true value within the error bars for all conditions and is thus not significantly affected by improper a priori assumptions on the albedo. In contrast, the AOD is significantly underestimated (by up to 18% for the retrieval at 360 nm) for $A < A_a$, and slightly overestimated for $A > A_a$. Systematic errors caused by incorrect assumptions on the albedo are largest at 360 nm.

[92] There are further possible sources for systematic errors not investigated here. First, MAX-DOAS instruments receive light scattered over a large horizontal distance (in particular at small elevation angles and high visibility). Therefore the measurements can be affected by horizontal inhomogeneities in the aerosol extinction profile, while a horizontally homogeneous atmosphere is assumed in the forward model. In particular, this can be a significant error source when measurements are performed at different azimuth directions. Second, a possible temperature dependence of the O₄ absorption might introduce systematic errors which cannot be quantified yet owing to the lack of data on the temperature dependence of the O₄ absorption cross section.

5. Conclusions and Outlook

[93] A new retrieval algorithm for the determination of properties of atmospheric aerosols using MAX-DOAS observations of the variation of the O₄ DOD and relative intensity with viewing direction has been presented. Based on model simulations using synthetic measurements, it has been shown that MAX-DOAS measurements of scattered sunlight contain substantial information on both the aerosol extinction profile and the optical/microphysical properties of particles in the lower troposphere.

[94] MAX-DOAS measurements of O₄ at a single absorption band already contain sufficient information to estimate the aerosol extinction in the lowermost 300 m of the atmosphere. To gain information on the aerosol extinc-

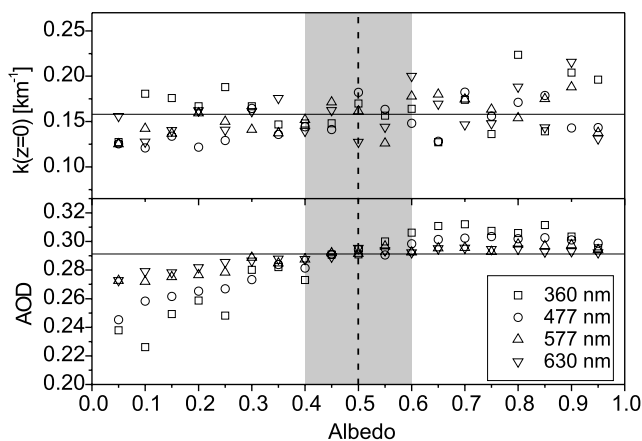


Figure 19. (top) Retrieved aerosol extinction at the surface and (bottom) aerosol optical depth as a function of the true surface albedo. Results are shown for retrievals using four different O₄ absorption bands as denoted in the legend. Horizontal lines indicate the true aerosol extinction and AOD. The dashed vertical line indicates the a priori surface albedo, and the gray area indicates the albedo a priori error.

tion profile at higher altitudes (up to $\approx 3 \text{ km}$), it is necessary to use measurements at several O₄ absorption bands and/or to consider the variation of the light signal with viewing direction. An important feature of the aerosol extinction profile retrieval is the increase in sensitivity for altitudes where the aerosol extinction is enhanced, which is a result of the nonlinearity of the problem. This means that aerosol layers (located either at the surface or at elevated levels), such as from biomass burning, industrial emissions or desert dust, can be detected very well by MAX-DOAS measurements.

[95] Including the variation of the observed intensity in the retrieval allows the AOD to be determined with a theoretical accuracy comparable to measurements from sky radiometers (in most cases better than 0.01). However, sky radiometers only yield information on aerosol properties over the total column, while MAX-DOAS observations allow for the first time substantial information on the vertical distribution of aerosols to be derived by passive remote sensing.

[96] MAX-DOAS measurements also contain substantial information on the optical and microphysical properties of aerosols, in particular if measurements are performed at different azimuth angles in the solar almucantar, a measurement geometry that is also used for the retrieval of the aerosol size distribution and complex refractive index by sky radiometers within the AERONET network, although the representation of the aerosol composition in the retrieval algorithm is still rather simplified: Only the fraction of the amount of one particle type a binary mixture of reflecting/absorbing and small/large particles is implemented so far. It has been demonstrated that the fraction of absorbing particles and the distinction between small and large particles can be determined with high accuracy by MAX-DOAS. There are several options for the representation of aerosol optical/microphysical properties in the retrieval algorithm,

which need to be investigated in the future. A simple approach is to represent the optical properties by three parameters only: the asymmetry parameter of a Henyey-Greenstein phase function [Henyey and Greenstein, 1941], the single scattering albedo and the Angström exponent [Angström, 1924]. A more sophisticated approach consists of retrieving the full angular dependence of the phase function instead of the asymmetry parameter.

[97] The determination of optical and microphysical aerosol properties requires measurements at several azimuth angles, with the best sensitivity gained from measurements in the aureole region of the sun. This requires a small field of view, a protection of the instrument against direct sunlight and the capability to perform automated measurements with varying azimuth angle. Since most of the current instruments do not have the capability to vary the azimuth angle automatically, further instrument development is necessary to meet these requirements.

[98] Compared to direct sunlight measurements by sky radiometers, the absolute precision of the AOD retrieved from MAX-DOAS measurements is likely to be limited by the systematic errors discussed in section 4.8, mostly owing to the more complex radiative transfer for scattered light compared to direct sunlight. The results presented in this paper are based on synthetic measurements, which means that it has been implicitly assumed that the observed quantities (O₄ DOD and intensity index) are correctly simulated by the radiative transfer model. Retrievals based on real MAX-DOAS measurements will reveal whether the radiative transfer can be correctly modeled, in particular regarding the question whether both the modeled intensities and the O₄ optical depths at different wavelengths can be simultaneously brought into agreement with the measurements.

[99] Sky radiometers rely on absolute radiometric measurements. Therefore instrument degradation is a source of systematic errors and a regular calibration of sky radiometers is necessary. In contrast, instrument degradation is not an issue for MAX-DOAS instruments which are based on measurements of relative quantities.

[100] Owing to the high variability of atmospheric aerosols, it is in most cases difficult to find appropriate a priori information. On the basis of simple assumptions on the temporal variability of aerosols, it has been shown in section 4.4 that this problem can be solved by using a Kalman smoother.

[101] The retrieval of aerosol properties can potentially be further improved by considering additional quantities measured by MAX-DOAS instruments. The magnitude of the Ring effect [Grainger and Ring, 1962] is determined by the amount of inelastic Raman scattering and thus contains information on atmospheric aerosols [Wagner et al., 2004]. The polarization characteristics of Rayleigh and Mie scattered light is different, which can be used to gain additional information on the relative contribution of Mie scattering and thus on atmospheric aerosols by equipping the MAX-DOAS instrument with a polarization filter. Furthermore, measurements of the oxygen A-band could provide information on the vertical distribution of aerosols at higher altitudes. Finally, absolutely radiometrically calibrated MAX-DOAS instruments would further increase the information content of this technique.

[102] The inverse model presented here can be easily adapted for the retrieval of vertical profiles of the numerous tropospheric trace gases detectable by MAX-DOAS instruments (e.g., NO₂, HCHO, BrO, IO, H₂O). Since the forward model is linear in case of optically thin absorbers, the profile retrieval can be performed in a single iteration. Therefore the numerical effort is much smaller than for the aerosol retrieval. As already described by Heckel et al. [2005] and Sinreich et al. [2005], the interpretation of MAX-DOAS measurements can be performed in a self-consistent way: In a first step, properties of atmospheric aerosols based on measurements of O₄ and intensity index are retrieved, which then serve as input for the inverse modeling of the vertical distribution of atmospheric trace gases.

[103] **Acknowledgment.** This work has been partly funded by the European Union (project EVERGREEN, grant EVG2-2001-00051).

References

- Angström, A. (1924), Solar and terrestrial radiation, *Q. J. R. Meteorol. Soc.*, **50**, 121–125.
- Backus, G. E., and J. F. Gilbert (1970), Uniqueness in the inversion of inaccurate gross Earth data, *Philos. Trans. R. Soc.*, **266**, 123–192.
- Barret, B., M. D. Maziere, and P. Demoulin (2002), Retrieval and characterization of ozone profiles from solar infrared spectra at the Jungfraujoch, *J. Geophys. Res.*, **107**(D24), 4788, doi:10.1029/2001JD001298.
- Berk, A., L. S. Bernstein, and D. C. Robertson (1989), MODTRAN: A moderate resolution model for LOWTRAN 7, *Tech. Rep. ADA214337*, Geophys. Dir., Phillips Laboratory, Kirtland Air Force Base, N. M.
- Bobrowski, N., G. Hönninger, B. Galle, and U. Platt (2003), Detection of bromine monoxide in a volcanic plume, *Nature*, **423**, 273–276.
- Charlson, R. J., S. E. Schwartz, J. M. Hales, R. D. Cess, J. A. Coakley Jr., J. E. Hansen, and D. J. Hofmann (1992), Climate forcing by anthropogenic aerosol, *Science*, **255**, 423–430.
- Dubovik, O., and M. D. King (2000), A flexible inversion algorithm for retrieval of aerosol optical properties from Sun and sky radiance measurements, *J. Geophys. Res.*, **105**, 20,673–20,696.
- Dubovik, O., A. Smirnov, B. N. Holben, M. D. King, Y. J. Kaufman, T. F. Eck, and I. Slutsker (2000), Accuracy assessments of aerosol optical properties retrieved from Aerosol Robotic Network (AERONET) Sun and sky radiance measurements, *J. Geophys. Res.*, **105**, 9791–9806.
- Ferlemann, F., N. Bauer, R. Fitzenberger, H. Harder, H. Osterkamp, D. Perner, U. Platt, M. Schneider, P. Vradelis, and K. Pfeilsticker (2000), Differential optical absorption spectroscopy instrument for stratospheric balloonborne trace-gas studies, *Appl. Opt.*, **39**, 2377–2386.
- Frieß, U., T. Wagner, I. Pundt, K. Pfeilsticker, and U. Platt (2001), Spectroscopic measurements of tropospheric iodine oxide at Neumayer station, Antarctica, *Geophys. Res. Lett.*, **28**, 1941–1944.
- Frieß, U., J. Hollwedel, G. König-Langlo, T. Wagner, and U. Platt (2004), Dynamics and chemistry of tropospheric bromine explosion events in the Antarctic coastal region, *J. Geophys. Res.*, **109**, D06305, doi:10.1029/2003JD004133.
- Grainger, J. F., and J. Ring (1962), Anomalous Fraunhofer line profiles, *Nature*, **193**, 762.
- Greenblatt, G. D., J. J. Orlando, J. B. Burkholder, and A. R. Ravishankara (1990), Absorption measurements of oxygen between 330 and 1140 nm, *J. Geophys. Res.*, **95**, 18,577–18,582.
- Haley, C. S., S. M. Brohede, C. E. Sioris, E. Griffioen, D. P. Murthag, I. C. McDade, P. Eriksson, E. J. Llewellyn, A. Bazureau, and F. Goutail (2004), Retrieval of stratospheric O₃ and NO₂ profiles for Odin Optical Spectrograph and Infrared Imager System (OSIRIS) limb-scattered sunlight measurements, *J. Geophys. Res.*, **109**, D16303, doi:10.1029/2004JD004588.
- Hansen, J., M. Sato, and R. Ruedy (1997), Radiative forcing and climate response, *J. Geophys. Res.*, **102**, 6831–6864.
- Heckel, A., A. Richter, T. Tarsu, F. Wittrock, C. Hak, I. Pundt, W. Junkermann, and J. P. Burrows (2005), MAX-DOAS measurements of formaldehyde in the Po-Valley, *Atmos. Chem. Phys.*, **5**, 909–918.
- Hendrick, F., et al. (2004), Retrieval of nitrogen dioxide stratospheric profiles from ground-based zenith-sky UV-visible observations: Validation of the technique through correlative comparisons, *Atmos. Chem. Phys.*, **4**, 2091–2106.
- Henyey, L. C., and J. L. Greenstein (1941), Diffuse radiation in the Galaxy, *Astrophys. J.*, **93**, 70–83.

- Hönninger, G., and U. Platt (2002), The role of BrO and its vertical distribution during surface ozone depletion at Alert, *Atmos. Environ.*, *36*, 2481–2489.
- Hönninger, G., C. von Friedeburg, and U. Platt (2004), Multi axis differential absorption spectroscopy (MAX-DOAS), *Atmos. Chem. Phys.*, *4*, 231–254.
- Hoogen, R., V. V. Rozanov, and J. P. Burrows (1999), Ozone profiles from GOME satellite data: Algorithm description and first validation, *J. Geophys. Res.*, *104*, 8263–8280.
- Houghton, J. T., Y. Ding, D. J. Griggs, M. Nouger, P. J. van der Linden, and D. Xiaosu (Eds.) (2001), *Climate Change 2001: The Scientific Basis—Contribution of Working Group I to the Third Assessment Report of the Intergovernmental Panel on Climate Change (IPCC)*, 944 pp., Cambridge Univ. Press, New York.
- Kalman, R. E. (1960), A new approach to linear filtering and prediction problems, *Trans. ASME J. Basic Eng.*, *82*, 35–45.
- Kneizys, F. X., E. P. Shettle, L. W. Abreu, J. H. Chetwynd, G. P. Anderson, W. O. Gallery, J. E. A. Selby, and S. A. Clough (1988), Users guide to LOWTRAN 7, *Tech. Rep. AFGL-TR-88-0177*, Air Force Geophys. Lab., Hanscom Air Force Base, Mass.
- Leser, H., G. Hönninger, and U. Platt (2003), MAX-DOAS measurements of BrO and NO₂ in the marine boundary layer, *Geophys. Res. Lett.*, *30*(10), 1537, doi:10.1029/2002GL015811.
- Levenberg, K. (1944), A method for the solution of certain non-linear problems in least squares, *Q. Appl. Math.*, *2*, 164–168.
- Marquardt, D. W. (1963), An algorithm for least-squares estimation of nonlinear parameters, *J. Soc. Ind. Math.*, *11*, 431–441.
- Platt, U. (1994), Differential optical absorption spectroscopy (DOAS), in *Air Monitoring by Spectroscopic Techniques*, vol. 127, pp. 27–83, John Wiley, Hoboken, N. J.
- Press, W. H., B. P. Flannery, S. A. Teukolsky, and W. T. Vetterling (1988), *Numerical Recipes in C*, Cambridge Univ. Press, New York.
- Preston, K. E., R. L. Jones, and H. K. Roscoe (1997), Retrieval of NO₂ vertical profiles from ground-based UV-visible measurements—Method and validation, *J. Geophys. Res.*, *102*, 19,089–19,097.
- Rodgers, C. D. (1990), The characterization and error analysis of profiles retrieved from remote sounding instruments, *J. Geophys. Res.*, *95*, 5587–5595.
- Rodgers, C. D. (2000), *Inverse Methods for Atmospheric Sounding: Theory and Practice*, Ser. Atmos. Oceanic Planet. Phys., vol. 2, edited by F. W. Taylor, World Sci., Hackensack, N. J.
- Rozanov, A. V., V. V. Rozanov, and J. P. Burrows (2000), Combined differential-integral approach for the radiation field computation in a spherical shell atmosphere: Nonlimb geometry, *J. Geophys. Res.*, *105*, 22,937–22,942.
- Rozanov, A., V. Rozanov, and J. P. Burrows (2001), A numerical radiative transfer model for a spherical planetary atmosphere: Combined differential-integral approach involving the Picard iterative approximation, *J. Quant. Spectrosc. Radiat. Transfer*, *69*, 491–512.
- Rozanov, A., H. Bovensmann, A. Bracher, S. Hrechanyy, V. Rozanov, B.-M. Sinnhuber, F. Strohm, and J. P. Burrows (2005), NO₂ and BrO vertical profile retrieval from SCIAMACHY limb measurements: Sensitivity studies, *Adv. Space Res.*, *36*, 846–854, doi:10.1016/j.asr.2005.03.013.
- Schofield, R., B. J. Connor, K. Kreher, P. V. Johnston, and C. D. Rodgers (2004), The retrieval of profile and chemical information from ground-based UV-visible spectroscopic measurements, *J. Quant. Spectrosc. Radiat. Transfer*, *86*, 115–131.
- Seinfeld, J. H., and S. N. Pandis (1998), *Atmospheric Chemistry and Physics*, 1126 pp., John Wiley, Hoboken, N. J.
- Sinreich, R., U. Friß, and U. Platt (2005), Multi axis differential optical absorption spectroscopy (MAX-DOAS) of gas and aerosol distributions, *Faraday Discuss.*, *130*, doi:10.1039/b419274p.
- Tegen, I., and A. A. Lacis (1996), Modeling of particle size distribution and its influence on the radiative properties of mineral dust aerosol, *J. Geophys. Res.*, *101*, 19,237–19,244.
- van Roozendaal, M., C. Fayt, P. Post, C. Hermans, and J.-C. Lambert (2003), Retrieval of BrO and NO₂ from UV-visible observations, in *Sounding the Troposphere From Space: A New Era for Atmospheric Chemistry*, edited by P. Borell et al., pp. 155–156, Springer, New York.
- Wagner, T., C. von Friedeburg, M. Wenig, C. Otten, and U. Platt (2002), UV-visible observations of atmospheric O₄ absorptions using direct moonlight and zenith-scattered sunlight for clear-sky and cloudy sky conditions, *J. Geophys. Res.*, *107*(D20), 4424, doi:10.1029/2001JD001026.
- Wagner, T., B. Dix, C. von Friedeburg, U. Friß, S. Sanghavi, R. Sinreich, and U. Platt (2004), MAX-DOAS O₄ measurements: A new technique to derive information on atmospheric aerosols—Principles and information content, *J. Geophys. Res.*, *109*, D22205, doi:10.1029/2004JD004904.
- Wittrock, F., H. Oetjen, A. Richter, S. Fietkau, T. Medeke, A. Rozanov, and J. P. Burrows (2004), MAX-DOAS measurements of atmospheric trace gases in Ny-Ålesund—Radiative transfer studies and their application, *Atmos. Chem. Phys.*, *4*, 955–966.

U. Friß, U. Platt, R. Sinreich, and T. Wagner, Institute for Environmental Physics, University of Heidelberg, Im Neuenheimer Feld 229, D-69120 Heidelberg, Germany. (udo.friess@iup.uni-heidelberg.de; ulrich.platt@iup.uni-heidelberg.de; roman.sinreich@iup.uni-heidelberg.de; thomas.wagner@iup.uni-heidelberg.de)

P. S. Monks and J. J. Remedios, Space Research Centre, University of Leicester, University Road, Leicester LE1 7RH, UK. (p.s.monks@leicester.ac.uk; jjr8@leicester.ac.uk)

A. Rozanov, Institute of Environmental Physics, University of Bremen, P.O. Box 33 04 40, D-28334 Bremen, Germany. (alex@iup.physik.uni-bremen.de)